ADAPTIVE ANTENNA ARRAYS APPLIED TO POSITION LOCATION

by
Donald F. Breslin

Thesis submitted to the Faculty of the
Virginia Polytechnic Institute and State University
in partial fulfillment of the requirements for the degree of

MASTER OF SCIENCE
in
The Bradley Department of Electrical and Computer Engineering

Approved:

Dr. Jeffrey H. Reed
(Chairman)

Dr. Timothy Pratt

Dr. Brian D. Woerner

August 1997
Blacksburg, Virginia

Adaptive Antenna Arrays Applied to Position Location

by

Donald F. Breslin

Committee Chairman: Dr. Jeffrey H. Reed

The Bradley Department of Electrical and Computer Engineering

Abstract

Wireless communication has enjoyed explosive growth over the past decade. As demands for increased capacity and quality grow, improved methods for harnessing the multipath wireless channel must be developed. The use of adaptive antenna arrays is one area that shows promise for improving capacity of wireless systems and providing improved safety through position location capabilities. These arrays can be used for interference rejection through spatial filtering, position location through direction finding measurements, and developing improved channel models through angle of arrival channel sounding measurements. This thesis provides an overview of the technical challenges involved in position location of wireless users and details the hardware development of a multi-sensor testbed at the Mobile and Portable Radio Research Group at Virginia Tech. This testbed is to be used for position location experiments as well as a host of other adaptive signal processing applications.

Acknowledgements

I would like to thank my advisor, Dr. Jeff Reed, for the invaluable support, guidance, and encouragement he has provided me during my research. I would also like to thank my committee members, Dr. Timothy Pratt and Dr. Brian Woerner, for reviewing this thesis and providing the necessary edits.

The hardware development effort that is the heart of this thesis would not have been possible without the assistance of key former and current members of MPRG including but not limited to Francis Dominique, Nitin Mangalvedhe, Steve Nicoloso, Paul Petrus, and the entire MPRG staff.

I am grateful to Dr. Scott Seidel for giving me the opportunity to take time off from my graduate research and gain valuable experience in industry. His work ethic and insight have been inspiring for me. I am also grateful to Dr. Joe Liberti for his guidance while at MPRG and for introducing me to the exciting area of adaptive antenna arrays.

I wish to deeply thank my parents for all of their support, guidance, and patience over the years. I thank God for looking over me during these past years and for granting me the ability to complete this degree.

Contents

List of Tables

List of Figures

Chapter 1

Introduction

1.1 Motivation

Wireless communication has enjoyed explosive growth over the past decade. As demands for increased capacity and quality grow, improved methods for harnessing the multipath wireless channel must be developed. One area driving research is public demand for improved safety using wireless communications. An exciting example is the ruling by the Federal Communications Commission (FCC) in June of 1996 that wireless service providers must provide position location information for mobile users who make use of the emergency Enhanced-911 (E-911) system. The ability to locate a mobile user within the 125 m RMS accuracy mandated by the FCC provides tremendous technical challenges for cellular and PCS service providers due to multipath channel conditions and multiple-access interference inherent to these wireless systems. This thesis provides a brief overview of position location for wireless users, introduces the fundamentals of adaptive antenna arrays and how they can be used for direction finding, and details the hardware development of a multi-sensor testbed at the Mobile and Portable Radio Research Group at Virginia Tech. This testbed is to be used for position location experiments as well as a host of other adaptive signal processing applications.

1.2 Objective and Outline of Thesis

The aim of this research is twofold. The first aim is to provide an overview of position location of wireless phones and specifically how adaptive arrays can be used for direction finding measurements. Secondly, this thesis details the development of a multi-sensor testbed that can be used for position location experiments involving direction finding with adaptive antenna arrays. The testbed, however, is intended for a host of applications such as adaptive beamforming for interference rejection, diversity analysis, and channel sounding for the development of improved channel models that incorporate angle of arrival characteristics.

The thesis is organized into seven chapters. Chapter 2 provides an overview of position location and the approaches that are available, covering the Global Positioning System as well as two different approaches to passive cellular geolocation. These approaches are based on determining either the time difference of arrival of a mobile's signal at three or more base stations or determining the angle of arrival of a mobile's signal at two or more base stations. Chapter 3 introduces the fundamentals of adaptive antenna arrays, the basics of adaptive beamforming with arrays, and an introduction to the MUSIC algorithm for direction of arrival estimation.

Chapter 4 covers the design of the multi-sensor testbed at MPRG, which mainly entails the design considerations in matching an analog RF front end to an analog to digital converter. Also covered is the digital signal processing done to convert the digitized band to complex baseband inputs to the DSP. Chapter 5 details the implementation issues of this hardware development effort, describing details such as the interfacing of the separate portions of the receiver. Chapter 6 covers a series of performance tests conducted to determine the Spurious Free Dynamic Range of the analog front end of the receivers. Chapter 7 concludes the thesis by covering the potential applications of the testbed and outlining the steps for calibrating the array for direction finding experiments.

Chapter 2

Position Location Overview

2.1 Motivation

Position location technologies have traditionally been of interest to the military and intelligence communities. In addition to the traditional applications of position location technologies, two new commercial applications have spurred research in this area: the use of position location technology for vehicle MAYDAY services and position location for mobile phones dialing 911 under the Enhanced-911 standard. The development of position location technologies for mobile phones has been prompted by the Federal Communications Commission's (FCC) requirement that wireless service providers, such as cellular, specialized mobile radio, and the newly allocated personal communications services, be able to determine the location of mobile phone users dialing 911. The development of MAYDAY vehicular services, on the other hand, has come from both government sponsored research into Intelligent Vehicle-Highway Systems (IVHS) and commercial applications such as vehicle Location and Monitoring Services (LMS) for trucking services and rental car agencies.

The use of position location for MAYDAY services has received much attention since 1991 when Congress passed the Intermodal Surface Transportation Efficiency Act (ISTEA), which make a national priority the development of an Intelligent Vehicle-Highway infrastructure. The US Department of Transportation (USDOT) as well as numerous State DOTs have funded research into and are conducting operational tests of MAYDAY services including position location of vehicles in need of emergency and non-emergency services. Many of these proposed MAYDAY systems

rely on the use of the Global Positioning System (GPS) developed by the US Government for military and civilian satellite-aided navigation. This system of 24 medium earth orbit satellites provides users with position location information that can be relayed to the appropriate service providers if the driver is in need of assistance. Relaying the driver's position is usually done over the existing cellular network but alternatively can be done via commercial satellite communications systems, which offer nearly global coverage.

Many operational tests have been performed by state DOTs in collaboration with industry to demonstrate MAYDAY technologies. The simplest of these has been the deployment of wireless call boxes along major roadways such as the Pennsylvania Turnpike and the San Diego SMART Call Box operational test. These call boxes require motorists to stop and notify authorities of traffic incidents. Other more automated MAYDAY operational tests include onboard crash sensors coupled with a GPS receiver and cellular data modem such as the Calspan Automatic Collision Notification System demonstrated in New York State, the Colorado MAYDAY system, Minnesota MAYDAY Plus, and the PUSHME MAYDAY System in Washington State. Automotive manufacturers such as Ford and GM have also implemented emergency position location using GPS and a cellular modem such as the Ford Rescu System introduced in the 1996 Lincoln Continental and GM Onstar introduced in the 1997 Cadillacs. Since cellular phone usage is common in automobiles and is growing rapidly, several cellular service providers have pursued cellular geolocation as a means of traffic monitoring and accident notification. The Cellular Applied to IVHS Tracking and Position Location (CAPITAL) project by ERA Inc. in the Washington DC area and TruePosition by the Associated Group Inc. and Comcast Cellular Communications Inc. on the New Jersey Turnpike are two examples of cellular geolocation applied to traffic monitoring and accident notification.

The desire by the public for security and safety has fueled much of the rapid growth in the cellular market. Over 18 million emergency calls were made in 1996 using wireless communications, and this number as well as the number of mobile phone subscribers is growing at an exponential rate [1]. Emergency 911 services for cellular telephones, however, has lagged behind that of wireline phones. For example, wireline phone Enhanced 911 (E-911) service allows for address determination, automatic callback, and text teletype (TTY) device usage, which are not currently available with

wireless 911 calls. The lack of these features has led to problems in responding to emergency calls particularly when mobile phone users do not know their exact location [2].

The FCC solicited comments regarding the support of E-911 by wireless service providers as well as private branch exchange phone systems in the last quarter of 1994 [3]. In response the Cellular Telephone Industry Association (CTIA) and the three principal public safety organizations, the National Emergency Number Association (NENA), the National Association of State Nine One One Administrators (NASNA), and the Association of Public Safety Communications Officials (APCO), filed a joint response urging the FCC to adopt a two phase plan for the deployment of E-911 services for mobile phone users and to provide guidelines to the position location requirement [1].

Phase I of the two phase plan endorsed by the CTIA and public safety organizations calls for the cell site and phone number of any commercial mobile radio service subscriber dialing 911 to be passed to the public service answering point (PSAP) as well as for access for the speech and hearing impaired using TTY devices. The cell site of the user is determined by the serving base station and is not expected to provide absolute position location for the user. This phase is expected to be completed withing 12 to 18 months of the FCC's final rule adoption.

Phase II calls for the automatic location in two dimensions of the wireless caller's position with a root mean square (RMS) accuracy of less than 125 m. This information will be passed on to the PSAP as with the user's phone number. The RMS accuracy is defined as

$$RMS = \sqrt{\varepsilon} = \sqrt{\mathbf{E}[(xa - xe)^2 + (ya - ye)^2]} \tag{2.1}$$

where xa is the actual longitude, ya is the actual latitude, xe is the estimated longitude, ye is the estimated latitude, and E[] is the expectation operator. In practice the expectation operator is replaced by the mean value over a set of position estimates. If the estimates of the x and y coordinates were striclty Gaussian in nature, the radial distance error would follow a Rayleigh distribution with 63 % of the estimates within the RMS point of the distribution. The CTIA proposed that the 125 m RMS accuracy be met roughly 70 % of the time. Phase II is expected to be completed within five years of the final ruling by the FCC.

The technology for performing this position location has not been specified by the Consensus group and a number of technologies are feasible for obtaining the user's position. Determination of the time difference of arrival (TDOA) of the mobile user's signal at multiple base stations provides postion location through triangulation methods. Alternatively, the angle of arrival (AOA) of the user's signal at multiple base stations also allows the user's location to be determined. A combination of these two methods has also been proposed for improved accuracy [4]. The advantage of these techniques over the mobile determining its position, with a GPS receiver for instance, and relaying this to the base station is that no modifications need to be made to current mobile phones. Thus, the burden of position location falls on the service provider, and no additional hardware such as a GPS receiver is required of the mobile user.

In June 1996, the FCC adopted a Report and Order [5] that creates rules to govern the availability of Enhanced-911 for wireless services. The rules mostly follow the consensus agreement reached by the CTIA and the principal safety organizations, except the Enhanced 911 features must be implemented only after the service provider receives a request from the PSAP administrator stating that they are capable of receiving and utilizing the information and that a mechanism for recovering the costs of such a position location system is in place. Nonetheless, within 18 months the service providers must provide the ability to transfer the call-back number of the mobile and the geographic location of the serving base station along with the 911 call to the PSAP when an emergency call is made. Within five years the service provider must be able to provide the mobile's position in two dimensions with a radial accuracy of within 125 m in 67 % of all cases.

There is a potential for combining the MAYDAY and Cellular Geolocation applications. For instance, many accident reports on the nations roadways are made by "good samaritan" cellular phone users who witness the accident. Position location for mobile phone users would then provide the public safety organization with the location of the reported accident. Also, by observing the density of calls made along major roadways and determining the mobiles velocity, traffic conditions can be monitored via geolocation. However, geolocation does not provide automatic notification of emergencies, as with cars equipped with crash sensors in many of the proposed MAYDAY systems, and would be less effective in rural areas where traffic density

and cellular coverage is less. Alternatively, the approach many MAYDAY systems have taken, in which the vehicle determines its own location and relays this to the safety organization, could be applied to cellular geolocation. GPS receivers could be put in new handheld phones, and the user's location could be relayed to the public safety organization when a 911 call is made. This is unlikely, however, due to the current cost, size, and battery requirements of a GPS receiver integrated with a mobile phone. Furthermore, GPS does not perform well indoors or in dense urban areas where view to the satellites may be blocked by tall buildings.

2.2 Overview of the Global Positioning System

The Global Positioning System consists of a constellation of 24 low-earth orbit satellites that provide world wide coverage. The GPS satellites use precise atomic clocks onboard to control the frequency and modulation rate of their two L-band carriers. Each satellite has a unique identifying code so that users can determine from which satellite the received signals originated. The satellites send time stamps of when their codes pass through a particular phase state. Based on when the user's receiver detects that phase state in the received signal, the propagation delay and thus range from each visible satellite can be estimated. This estimate is termed the pseudorange. With accurate knowledge of the satellite's orbits and the user's range from each satellite, the user's position can be determined. If the user had a perfect clock, three visible satellites would be required to determine position in three dimensions. In practice, however, a lower accuracy clock is used by the observer, and the signal from a fourth satellite is used to correct clock errors. The required information describing the satellite's orbit (ephemeris data), the code phase state time stamps, and clock offset corrections is provided in the GPS navigation message on both of the satellite's signals.

All GPS satellites transmit signals on the same two carriers, L1 at 1575.42 MHz and L2 at 1227.6 MHz, using code division multipe access. The Coarse/Acquisition or C/A code modulates the L1 carrier at a 1.023 Mcps rate and is available for civilian use. The Precision or P code is encrypted into the Y code and modulates the L1 and L2 carriers at a rate of 10.23 Mcps. The P code is available only to authorized users. The navigation message is a 50 bps signal that is mixed with both

the C/A and P codes before carrier phase modulation. On the L1 carrier, the P code is used to modulate the inphase component and the C/A code is used to modulate the quadrature component, a method known as quadrature phase modulation.

The orthogonal C/A codes come from a class of codes known as Gold codes and repeat every 1023 chips (1 millisecond). The P code, on the other hand, is designed to repeat every 280 days although a new key is normally sent to the code generators before this occurs. Due to the length of time required to synchronize to such a long code, the C/A code, as the name implies, is used to aid in coarse acquisiton of the P code for authorized users.

The Department of Defense (DOD) allows only the C/A code to be used for commercial systems and all timing reference for commercial systems are made with respect to this lower precision code. Furthermore, the US government dithers the timing of the C/A code to limit the accuracy for commercial users of the system. This limitted accuracy for commercial users is termed selective availability. Accuracies in horizontal coordinates of 100 m rms are attainable with commercial GPS with selective availability as compared to accuracies within 18 m rms using the Precision code. However, the DOD has announced its intention to stop the dithering of the C/A code and hence increase accuracy. In the mean time, this selective availability of the code has been circumvented through the use of differential GPS. In differential GPS a local base station with a known location receives the GPS signal, determines the error in its estimated position and transmits correction factors for the satellites, usually over FM-subcarriers, to differential GPS receivers so that more accurate positions can be calculated with commercial GPS.

2.3 Overview of Cellular Geolocation

Cellular geolocation refers to the location of mobile phones by observing and comparing the signal received by the mobile phone at multiple base stations. Two approaches for determining the mobile's position include determining the relative time difference of arrival (TDOA) and determining the angle of arrival (AOA) of the mobile's signal at multiple base stations.

By determining the time difference of arrival of a mobile's signal at two base stations the mobile's position can be fixed to a hyperbola with the two base stations as

the foci. Every location on the hyperbola will have the same observed time difference of arrival at the given base stations. With two sets of time difference of arrival measurements, requiring three base stations, the mobile's position can be estimated as the intersection of the two hyperbolas. This method is thus referred to as hyperbolic position location[Reference]. The time difference of arrival can be found by the generalized cross correlation method or one of many variations of this technique. This essentially consists of taking the recorded and time stamped signal from each base station and sliding the two versions of the signal past each other in time. A correlation peak will occur when the two copies of the signal are exactly aligned in time and by subtracting the time of arrival from each record a relative time difference of arrival can be determined for the mobile's signal at the two base stations. Mulitpath conditions and weak signal to noise ratio (SNR) can seriously degrade the TDOA estimation accuracy based on the cross-correlation approach. In addition, since the mobile's signal must be captured by non-serving adjacent cell base stations, the co-channel reuse distance is decreased for the user at the non-serving base stations. This can result in relatively high co-channel interference levels. TDOA based position location requires a single omnidirectional receive antenna and a dedicated tunable receiver with an accurate time reference at the base stations.

A key issue for TDOA approaches is accurate timing and proper synchronization between base stations. For example, an error of 100 ns in the TDOA estimate can translate into a range error of 30m. Stable atomic clocks such as cesium standards can be used for accurate timing, but periodic synchronization still must be performed for all base stations in the service area. A less expensive approach is to base the timing information on the GPS time standard. An HP5071 Cesium standard costs approximately $ 50,000 whereas a GPS based disciplined oscillator from the HP58000 series costs approximately $ 5,000 and has a comparable timing accuracy to the cesium standard of within 110 ns when locked to the GPS signal.

The angle of arrival approach uses antenna arrays at the base station to determine the direction from which the mobile's signal arrives. Tracing a signal along this line of bearing from the known base station location for two or more base stations provides an intersection that is the estimate of the mobile's position. Numerous techniques have been developed to determine the angle of arrival of signals incident on an antenna array. These methods typically are based on the phase difference of the signal at

adjacent elements in the antenna array since this phase difference is proportional to the angle of arrival of the incoming signal. Superresolution techniques have also been developed that take advantage of the structure of the input data model. These methods, including MUSIC and ESPRIT, fall into a class of algorithms known as subspace-based techniques [6].

These methods require an antenna array with all the associated cabling to be mounted at the base stations and a dedicated receiver capable of performing direction finding. The required hardware for the AOA approach is thus more complex and expensive and requires more room on the cellular towers for the antenna array and cabling than the single antenna TDOA approach.

A second key issue for both TDOA and AOA approaches, termed "hearability," is the number of base stations that can detect the mobile's signal. In addition to the serving base station, which handles the mobile's emergency call, secondary base stations must be able to detect and record or perform direction finding on the mobile's signal. Since the mobile will be outside the designed coverage area or cell of the secondary base stations, its signal may be very weak, and thus a low signal to noise ratio (SNR) can be expected at these secondary base stations. Furthermore, relatively high interference levels are possible at the secondary base stations compared to the serving base station since the frequency reuse distance is decreased. In other words, the secondary base station will be closer to the next base station reusing the mobile's channel than the serving base station.

A hybrid approach to cellular geolocation can be applied by combining both TDOA and AOA techniques. In this case the gain of an adaptive antenna array can improve the SNR at the secondary base stations for improved TDOA estimation compared to omnidirectional receive antennas and direction finding can be performed at the same time. This combination eases the hearability requirement since with only two receiving base stations, two lines of bearing and a TDOA hyperbola can be determined and a position location estimate made.

Chapter 3

Adaptive Antenna Array Overview

3.1 Fundamentals of Antenna Arrays

An antenna array is a set of antenna elements arranged in space whose outputs are combined to give an overall antenna pattern that can differ from the pattern of the individual elements. An array can achieve the same directional performance of a larger antenna by trading the electrical problems of combining several antenna outputs for the mechanical problems of supporting and turning a large antenna. By varying the phase and amplitude of the individual element outputs before combining, the overall array pattern can be steered in the desired user's direction without physically moving any of the individual elements.

The overall radiation pattern of an array is determined by the radiation pattern of the individual elements, their positions, orientations in space, and the relative phase and amplitudes of the feeding currents to the elements. By the principle of pattern multiplication, the overall radiation pattern $F(\omega, \Theta, \phi)$ is found as the product of the individual element radiation patterns $g(\omega, \Theta, \phi)$ with the array factor $f(\omega, \Theta, \phi)$

$$F(\omega, \Theta, \phi) = g(\omega, \Theta, \phi) f(\omega, \Theta, \phi) \tag{3.1}$$

The array factor is in turn determined by the relative positions of the elements in space as well as the relative phase and amplitude levels of the feeding currents to the elements. The array factor, and thus the overall pattern of the array, can be

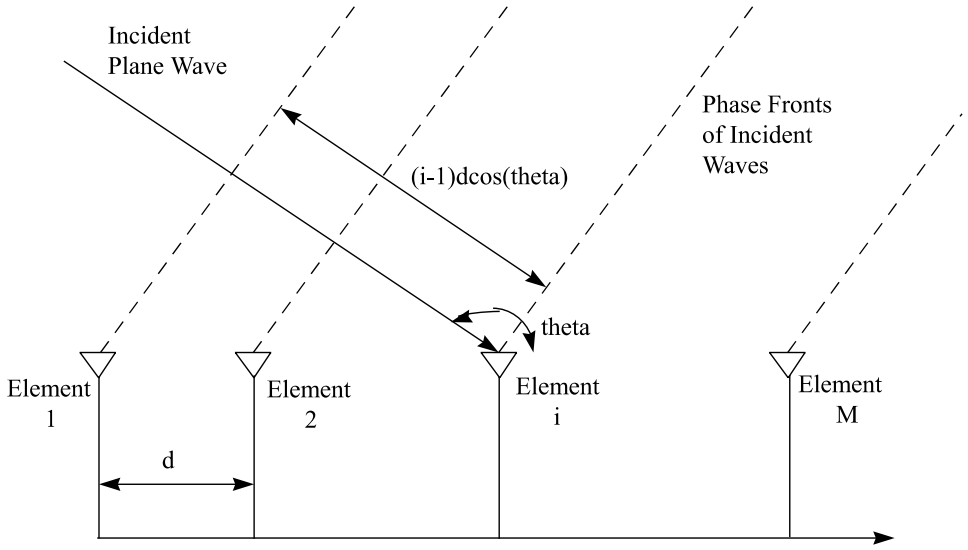

Figure 3.1: Phase Relationship of Currents for a Plane Wave Incident on a Uniform Linear Array

continuously scanned or adapted by adjusting the relative phase and amplitude levels between the currents at the elements [7].

One of the simplest geometries for an array is a linear array in which the centers of the antenna elements are aligned along a straight line. If all of the centers of the elements lie in a plane, the array is a planar array. Examples include the linear array, a circular array, and arbitrarily shaped planar arrays. For the uniformly spaced linear array, the diagram below shows the phase relationship between the currents generated at the elements for the given angle of arrival Θ measured from the principal axis of the array. Since the signal present at element two has traveled a distance $d\cos(\Theta)$ farther than the signal present at element one, its phase will lag behind that of element one by $\beta d\cos(\Theta)$ where $\beta = 2\pi/\lambda$ is the phase propagation factor. This relation holds for a narrowband signal, in this case a signal whose modulated bandwidth is much less than the carrier frequency. The narrowband assumption allows us to assume that the only difference between the signal present at element two and element one is the phase shift induced by the extra distance traveled and is not significantly affected by the modulation during this time.

Consider a transmitted narrowband signal in complex envelope representation,

$$s(t) = u(t)exp[-j[\omega_o t + v(t)]] \tag{3.2}$$

where u(t) is the signal amplitude and ω_0 is the center frequency. For an array of isotropic elements, $g(\omega_o) = 1$, and taking the received signal at element one as the reference, the received signals $x_i(t)$ for a uniform linear array with element spacing d can be represented in matrix form as

$$\mathbf{x}(t) = \begin{bmatrix} 1 \\ exp[-j\beta dcos(\Theta)] \\ exp[-j\beta 2dcos(\Theta)] \\ \vdots \\ exp[-j\beta(N-1)dcos(\Theta)] \end{bmatrix} s(t) = \mathbf{a}(\Theta)s(t) \tag{3.3}$$

where N is the number of elements, Θ is the angle of arrival, and $\mathbf{a}(\Theta)$ is the steering vector. For simplicity, the frequency dependence of $\mathbf{a}(\omega_o, \Theta, \phi)$ has been dropped for the narrowband case, and the elevation angle ϕ is assumed to be zero relative to the element's boresight. The collection of the steering vectors for all angles (Θ, ϕ) for a given ω_o is known as the array manifold. The array manifold must be carefully measured to calibrate the array for direction finding experiments.

For narrowband adaptive beamforming, each element output x_i is multiplied by a complex weight w_i^*, modifying the phase and amplitude relation between the branches, and summed to give $y(t)$

$$y(t) = \begin{bmatrix} {w_1}^* & {w_2}^* & {w_3}^* & \cdots & {w_N}^* \end{bmatrix} \begin{bmatrix} 1 \\ exp[-j\beta dcos(\Theta)] \\ exp[-j\beta 2dcos(\Theta)] \\ \vdots \\ exp[-j\beta(N-1)dcos(\Theta)] \end{bmatrix} s(t) = \mathbf{w}^H\mathbf{x}(t). \tag{3.4}$$

Since the array factor for the overall antenna pattern is dependent on the phase and amplitude relationship between the branches and the weight vector modifies the phase and amplitude relationship, the overall array pattern can be continually modified by adjusting the weight vector. The overall pattern for the array is given by

$$F(\omega, \Theta, \phi) = |\mathbf{w}^H\mathbf{a}(\omega, \Theta, \phi)|. \tag{3.5}$$

For our narrowband uniform linear array of isotropic elements, the pattern becomes

$$F(\Theta) = \left| \begin{bmatrix} {w_1}^* & {w_2}^* & {w_3}^* & \cdots & {w_N}^* \end{bmatrix} \begin{bmatrix} 1 \\ exp[-j\beta dcos(\Theta)] \\ exp[-j\beta 2dcos(\Theta)] \\ \vdots \\ exp[-j\beta(N-1)dcos(\Theta)] \end{bmatrix} \right| = f(\Theta) \quad (3.6)$$

Note that since the element pattern is isotropic, $g(\omega_o) = 1$ for all Θ and ϕ, the overall pattern becomes the pattern created by the array factor. Including the element pattern for the array and using the pattern multiplication principle mentioned above leads to

$$F(\Theta, \phi) = g(\theta, \phi) f(\Theta). \quad (3.7)$$

Note that since the element pattern has a ϕ dependence this parameter is included in the overall pattern. The array factor in this case has no ϕ dependence due to the linear geometry chosen. More complicated array geometries can be used for variation of the pattern along ϕ as well.

3.2 Adaptive Beamforming and Spatial Filtering

Adaptive algorithms have traditionally been applied to time domain filtering in which the tap weights of an FIR filter are adapted to minimize an error based on some criteria. For a narrowband antenna array, the adaptation is applied to the complex weight vector, one weight per element. In a sense, the array can be considered as a means to sample the incoming waveforms in space as opposed to a temporal dimension. By adapting the weights and changing the array pattern, the algorithm attempts to minimize the error through spatial filtering as opposed to the time and frequency domain filtering done through adapting FIR filter tap weights. Adaptive beamforming can be used to separate users who occupy the same frequency band at the same time as long as they are spatially separated.

In discrete time where at time index k, $t = kT_s$, the input or illumination vector may be expressed as

$$\mathbf{x}_k = \begin{bmatrix} x_{0,k} & x_{1,k} & x_{2,k} & \cdots & x_{N-1,k} \end{bmatrix}^T. \quad (3.8)$$

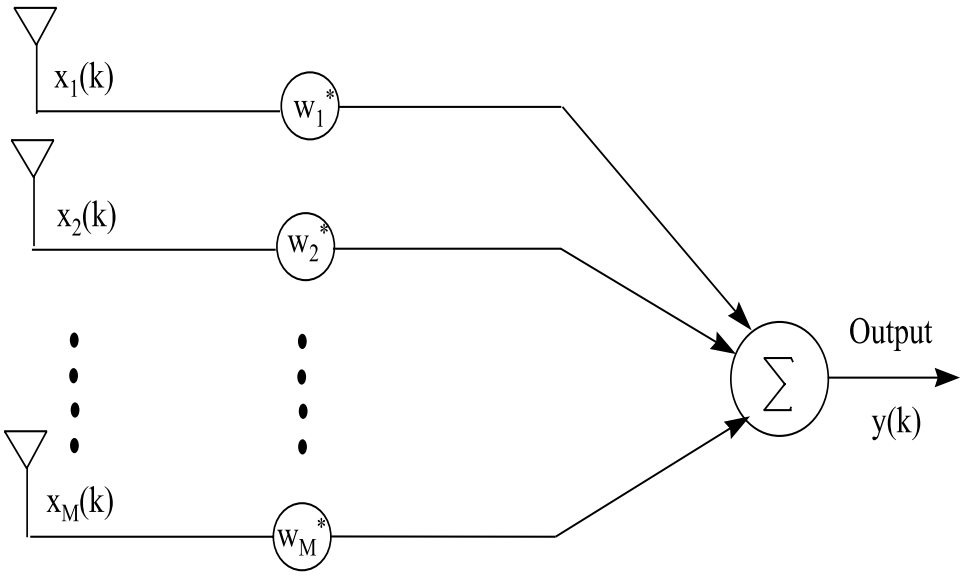

Figure 3.2: Narrowband Beamformer

The weight vector may be expressed as

$$\mathbf{w}_k = \begin{bmatrix} w_{0,k} & w_{1,k} & w_{2,k} & \cdots & w_{N-1,k} \end{bmatrix}^T. \tag{3.9}$$

This weight vector can be applied in the analog portion of a receiver using phase shifters and attenuators or in the digital domain after the signal has been digitized and filtered. One advantage of the digital approach is that the I and Q channels can be derived in the digital domain where perfectly quadrature mixers can be implemented. In the analog domain it is difficult to keep the local oscillator signals feeding the I and Q mixers perfectly 90 degrees out of phase. Thus, some component of the I channel will leak into the Q channel and vice versa. This quadrature misalignment is inevitable due to the inaccuracies of analog phase shifters.

For a narrowband array, the scalar output is given by the linear combination of the sampled inputs multiplied by the complex weights,

$$y_k = \mathbf{x_k}^H \mathbf{w_k} \tag{3.10}$$

where $()^H$ denotes the Hermitian transpose, which combines the transposition and conjugation operations.

For a wideband array, each complex weight is replaced by a tapped delay line to provide frequency response adaptation as well as spatial adaptation. Intuitively,

wider bandwidth signals may exhibit differing phase relationships from element to element across the signal passband due to the changing frequency. Wideband arrays provide further challenge in that the signal must be digitized at a higher sample rate to accomodate the full signal bandwidth. Finally, the array elements themselves must be sensitive across the signal passband for extremely wideband arrays.

Given knowledge of the original narrowband transmitted signal, the instantaneous error is determined from

$$\epsilon_k = d_k - y_k = d_k - \mathbf{x_k}^H \mathbf{w_k} \tag{3.11}$$

where d_k is the desired signal at the receiver, equal to the transmitted signal. The mean square error can be expressed as

$$MSE = E[{\epsilon_k}^2] = E[{d_k}^2] + \mathbf{w_k}^H \mathbf{R}_{xx} \mathbf{w}_k - 2\mathbf{r}_{xd}{}^H \mathbf{w}_k \tag{3.12}$$

where $\mathbf{R}_x x$ is the input correlation or covariance matrix and $\mathbf{r}_{xd}$ is the cross correlation matrix between the desired signal and the received signal. Based on this MSE an adaptive algorithm could be applied to minimize the error and thus improve the signal to interference and noise ratio at the receiver. Note that the error is a quadratic function of the weight vector. This guarantees that the error surface has a single global minimum, and thus one true optimum solution exists.

The optimum solution for minimizing the MSE is the Weiner-Hopf solution. This is found by taking the derivative of the MSE with respect to the weight vector and setting this equal to zero [Wid85]. It can be shown that this derivative or gradient in vector space is equal to

$$\Delta_k = 2\mathbf{R}_{xx}\mathbf{w}_k - 2\mathbf{r}_{xd} = 0. \tag{3.13}$$

Rearranging,

$$\mathbf{R}_{xx}\mathbf{w}_k = \mathbf{r}_{xd}. \tag{3.14}$$

Assuming $\mathbf{R}_{xx}$ is non-singular, the optimimum solution is found as

$$\mathbf{w}_k = \mathbf{R}_{xx}{}^{-1}\mathbf{r}_{xd}. \tag{3.15}$$

For stationary input data, the process only needs enough time to develop an adequate estimate of $\mathbf{R}_{xx}$ and $\mathbf{r}_{xd}$. Then $\mathbf{R}_{xx}{}^{-1}$ is computed, and the optimum weight vector is found. However, since matrix inversion is non-trivial, especially to implement on a

DSP, iterative techniques have been developed that are easier to implement and still arrive at the optimum solution in the limit. The update equation of these iterative approaches can generally be expressed as

$$\mathbf{w}_{k+1} = \mathbf{w}_k + \mu(-\Delta_k). \tag{3.16}$$

The stochastic gradient algorithms attempt to find the optimum solution by continually stepping in the negative direction of the gradient. Thus, they adjust the weight vector to move toward the minimum of the MSE surface where the optimum solution lies. The step size is controlled by the parameter μ. Different classes of algorithms take differing estimates of the gradient. One popular method is the LMS algorithm, which uses the instantaneous gradient to estimate the true gradient.

An important tradeoff exists in the proper choice of μ for the iterative approaches. A large step size allows the algorithm to update quickly but may also cause the estimate of the optimum solution to wander significantly after the algorithm has reached convergence. A smaller step size may be chosen to reduce this wandering but will require a longer time for the algorithm to reach the optimum solution. The proper choice depends on the propagation environment in which the array is intended to operate. If high mobility is to be supported, a larger μ is required than if the application is for nearly stationary users as with wireless links to the home. There are additional stability requirements on proper step size choice. The LMS algorithm is guaranteed to convergence to the optimum solution only if the step size satisfies

$$\frac{-1}{\lambda_{max}} < \mu < 0 \tag{3.17}$$

where λ_{max} is the maximum eigen value of the input covariance matrix $\mathbf{R_{xx}}$ [8].

3.3 Blind Adaptive Beamforming

The adaptation outlined above is based on the assumption that the desired signal is known at the receiver at the time the signal arrives. In practice this can be accomplished with a training sequence sent periodically over the RF channel. In this case the transmitter periodically sends a series of bits that are known in advance at the receiver. Thus, any distortion in the received training sequence is due to channel impairments such as multipath and interference. The received signal can then be filtered by adjusting taps in a tapped delay line or adjusting weights in a spatial filter to

force the received training sequence back to the known transmitted signal. This equalization counters the effects of multipath and interference in the channel. Adding a known training sequence leads to additional overhead, which limits the channel bandwidth available for data. An alternative is to demodulate the signal and, assuming the demodulator has made the correct choice, use the estimated received symbols as the desired signal. This approach, known as decision directed feedback, works well when the receiver can accurately estimate the received bit. In low signal to noise conditions, however, an incorrect symbol estimate for d_k can cause the algorithm to diverge from the optimum solution.

Another approach is to use a basic property of the signal or modulation itself to adapt the array. These property restoral algorithms are known as blind algorithms since they do not require a training sequence. A classic example is the Constant Modulus Algorithm (CMA) which adapts to restore the constant envelope property of FM, PM, and PSK signals. Other properties that can be exploited for adaptation are the finite alphabet property of digital signals or the property of cyclostationarity that exists in most modulated signals.

For CMA the error function is replaced by a cost function that measures the signal's deviation from the constant modulus property that the desired signal is known to have. The intuitive explanation is that unwanted amplitude modulation on the received signal is due to multipath, interference, and additive noise. Thus minimizing the envelope modulation will effectively filter out the interference and will seek to minimize the effects of multipath and noise.

The cost function takes the form

$$J(\mathbf{w}_k) = E[(|\mathbf{y}_k|^p - \delta^q)^q] \tag{3.18}$$

where p and q are positive integers and δ is the desired nominal value of the received signal envelope. Typically δ is set to 1, and the algorithm is referred to as the "p-q" form of CMA [9].

The gradient search algorithms from (3.16) can be used to iteratively minimize the above cost function. The instantaneous estimate of the gradient can be shown to be [10]

$$\Delta J = [(|\mathbf{y}_k|^2 - 1)]y_k^* \mathbf{x}_k \tag{3.19}$$

for p = 2, q = 1 and δ chosen to be 1. Using this gradient estimate in the update

equation yields the following iteration

$$\mathbf{w_{k+1}} = \mathbf{w_k} - \mu[(|\mathbf{y}_k|^2 - 1)]y_k^* \mathbf{x}_k. \tag{3.20}$$

This update equation can be simplified somewhat by defining an error term

$$\epsilon_k = [(|\mathbf{y}_k|^2 - 1)]y_k. \tag{3.21}$$

This allows equation (3.20) to be written as

$$\mathbf{w_{k+1}} = \mathbf{w_k} - \mu\epsilon_k^* \mathbf{x}_k. \tag{3.22}$$

This update equation can be compared to the complex version of the LMS algorithm except here the error term is derived based on the constant modulus property as opposed to comparing the received signal with the known sequence.

The blind adaptation algorithms such as CMA have the advantage that they don't require a training sequence to adapt. The CMA algorithm is known to converge to the strongest user in the channel. The CMA algorithm's convergence properties have been studied under various channel conditions [11]. In order to track multiple users in a single channel, the algorithm must be initialized for the weaker users in an appropriate manner given knowledge of the strongest user's spatial response. It has been shown that through initializing secondary CMA algorithms to orthogonal patterns to the strongest user, multiple targets can be acquired with this blind algorithm [12]. This approach does suffer somewhat in that the secondary algorithms may eventually converge to the strongest user if proper care is not taken to monitor the correlation of the secondary weight vectors with the primary user's weight vector as well as other secondary user's weight vectors.

3.4 Direction Finding

The Multiple Signal Classification (MUSIC) algorithm proposed by Schmidt in 1979 [13] is an algorithm for estimating a range of signal parameters including the number of incident signals and their direction of arrival (DOA). MUSIC is a subspace-based algorithm that exploits the eigen structure of the input covariance matrix. Other applications of MUSIC include estimating the frequency of sinusoids in low SNR conditions and time delay estimation of multipath channels. This algorithm has been implemented and tested in wireless channels [14].

The MUSIC algorithm takes a geometric view of the signal classification problem. For an M element array with D signals incident on the array, the received input data vector may be expressed as a linear combination of the D incident waveforms and noise.

$$\begin{bmatrix} x_1 \\ \vdots \\ x_M \end{bmatrix} = \begin{bmatrix} \mathbf{a}(\Theta_1) & \cdots & \mathbf{a}(\Theta_D) \end{bmatrix} \begin{bmatrix} s_1 \\ \vdots \\ s_D \end{bmatrix} + \begin{bmatrix} n_1 \\ \vdots \\ n_D \end{bmatrix} \tag{3.23}$$

$$\mathbf{x} = \mathbf{A}\mathbf{s} + \mathbf{n} \tag{3.24}$$

where $\mathbf{s}$ is the vector of incident signals, $\mathbf{n}$ is the noise vector, and $\mathbf{a}(\Theta_j)$ is the array steering vector corresponding to the direction of arrival of the jth signal. Viewing the received vector $\mathbf{x}$ and the steering vector $\mathbf{a}(\Theta_j)$ as vectors in M dimensional space, it can be seen that $\mathbf{x}$ is a particular linear combination of the array steering vectors with s_1 through s_D being the coefficients of the combination. Using this data model, the input covariance matrix $\mathbf{R}_x x$ can be expressed as

$$\mathbf{R}_x x = E[\mathbf{x}\mathbf{x}^H] = \mathbf{A}E[\mathbf{s}\mathbf{s}^H]\mathbf{A}^H + E[\mathbf{n}\mathbf{n}^H] \tag{3.25}$$

$$\mathbf{R}_x x = \mathbf{A}\mathbf{R}_{ss}\mathbf{A}^H + {\sigma^2}_{Noise}\mathbf{I} \tag{3.26}$$

where $\mathbf{R}_{ss}$ is the signal correlation matrix E[$\mathbf{s}\mathbf{s}^H$].

Given that the individual steering vectors are linearly independent, the matrix $\mathbf{A}$ has full column rank. Also, matrix $\mathbf{R}_{ss}$ will be non-singular as long as the incident signals are at most partially correlated. The matrix $\mathbf{A}\mathbf{R}_{ss}\mathbf{A}^H$ will then be positive semidefinite with rank D as long as the number of incident signals D is less than the number of array elements M. Using linear algebra, this means that M-D eigenvalues of matrix $\mathbf{A}\mathbf{R}_{ss}\mathbf{A}^H$ are zero. For eigenvalues λ_1, λ_2, ..., λ_M and eigenvectors ν_1, ν_2, ..., ν_M of matrix $\mathbf{R}_{xx}$, the M-D smallest eigenvalues are equal to ${\sigma^2}_{Noise}$. Estimating $\mathbf{R}_{xx}$ with a finite data sample can cause the eigenvalues corresponding to the noise power to not be identical. They will, however, appear as a tightly spaced cluster of eigenvalues with the variance decreasing as the number of data samples used to estimate $\mathbf{R}_{xx}$ increases. Once the multiplicity of the smallest eigenvalue is determined, the number of signals is given by

$$D = M - K \tag{3.27}$$

where M is the number of elements and K is the number of eigenvalues corresponding to the noise subspace. Based on the definition of eigenvalues and eigenvectors, the eigenvectors corresponding to the smallest eigenvalues satisfy

$$\mathbf{R}_{xx}\nu_i = \sigma^2{}_{Noise}\nu_i, fori = D+1, ..., M. \tag{3.28}$$

Observing (3.26), we see that

$$\mathbf{A}\mathbf{R}_{ss}\mathbf{A}^H\nu_i = 0, fori = D+1, ..., M. \tag{3.29}$$

Now note that since $\mathbf{A}$ is full column rank and $\mathbf{R}_{ss}$ is non-singular, it follows that

$$\mathbf{A}^H\nu_i = 0, fori = D+1, ..., M. \tag{3.30}$$

This implies that the column vectors of $\mathbf{A}$ are perpendicular to the eigenvectors ν_{D+1}, ..., ν_M corresponding to the noise.

In summary, the eigenvectors of the covariance matrix $\mathbf{R}_{xx}$ belong to one of two orthogonal subspaces, the principle eigen vector subspace corresponding to the signals and the non-principle eigen subspace termed the noise subspace. The steering vectors corresponding to the direction of arrival of the signals span the signal subspace and are thus orthogonal to the noise subspace. By determining the noise eigenvalues and eigenvectors, the noise subspace can be estimated. Then the array manifold can be searched to find the eigenvectors that are orthogonal to the noise subspace. The orthogonal eigenvectors are the steering vectors of the received signals, and thus their direction of arrival can be determined. The MUSIC spectrum can be expressed as

$$P_{MUSIC}(\Theta) = \frac{1}{\mathbf{a}^H(\Theta)\mathbf{P}_N\mathbf{P}_N^H\mathbf{a}(\Theta)} \tag{3.31}$$

where

$$\mathbf{P}_N = [\nu_{D+1}, ..., \nu_M] \tag{3.32}$$

is the collection of the noise eigenvectors. The matrix $\mathbf{P}_N\mathbf{P}_N^H$ is a projection matrix onto the noise subspace. For steering vectors that are orthogonal to the noise subspace, the denominator of (3.31) will become very small, and thus the peaks will occur in $P_{MUSIC}(\Theta)$ corresponding to the angle of arrival of the signal. When the ensemble average of the array input covariance matrix is known and the noise can be considered uncorrelated and identically distributed between the elements, the peaks

of the MUSIC spectrum are guaranteed to correspond to the true angle of arrival of the signals incident on the array. Thus, with perfect array calibration so that the true steering vectors are known exactly, the MUSIC algorithm can resolve arbitrarily closely spaced signals. This accuracy is limited however by the accuracy with which the array manifold can be measured and by whether the manifold changes slightly between array calibration and data collection.

Chapter 4

Glomo Receiver Hardware Design

4.1 Overview

This chapter describes the design procedure for the analog front end of the adaptive antenna array developed at MPRG. Performance specifications such as transmit and receive powers, receiver gain, and dynamic range are discussed. Choice of IF freuqency, sampling rate and bandwidth choices are also discussed. This chapter concludes with a suggested list of standard MiniCircuits components and analog filters to provide an analog front end for each of the antenna array elements.

This hardware development effort was funded by the Global Mobile Communications (GloMo) project. The GloMo project is a funded research effort sponsored by DARPA for the development of innovative spread spectrum modems. This contract has funded much of the Multi-Sensor Testbed hardware development. Two base station architectures have been investigated under GloMo as well as a less complex adaptive filter for a mobile transceiver.

One base station approach implements a multi-user receiver with two stages of interference cancellation. In this approach a single user receiver is implemented at the base for each mobile. Using the demodulated output of each receiver as the initial estimate of the user's signal, the estimate is then subtracted from all of the other users' signals. The result is used to estimate each user's signal again. This approach is resistant to unequal power levels once all of the users have been acquired. However it does require stringent power control during the acquisition phase.

As an alternative to the multi-user receiver, an adaptive antenna array has also

been implemented at the MPRG to separate users based on spatial filtering. With this approach, single user receivers are used at each output of the multi-target beamformer since the beamformer can provide interference cancellation by adaptively changing the array beampattern. The analog and digital hardware up to the DSP for both approaches will be identical. However, the adaptive array will have a complete analog and digital chain for each antenna element. The mobile receiver will also use the same analog and digital components but will implement adaptive digital filtering for interference cancellation on its DSP section.

The following sections describe the design of the analog portion of the receiver for each element up to the complex baseband input to the DSP. This design will, however, be duplicated for the multi-user base station and the mobile units. Initially, a half-duplex link will be implemented to show the multi-user capabilities of both base station approaches. In later stages a duplexer will be added to the front end, and a full-duplex link will be demonstrated using frequency division duplexing.

4.2 Performance Specifications

The adaptive array design for each element consists of two parts, an analog front end and a digital processing section. The purpose of the analog portion is to downconvert the signal present at each element from an RF frequency of 2050 MHz to an IF suitable for bandpass digitization. The RF frequency was chosen due to the availability of standard components at this frequency, the proximity to the PCS band, and the FCC license attained by MPRG to operate in this band. The digital portion performs a second stage of downconversion while decimating, filtering, and splitting the signal into I and Q quadrature format for complex baseband processing on a DSP. A block diagram of the receiver including the analog tuner is shown in the figure below.

Note that a single receiver is shown in the diagram. For the eight element array the analog tuner and digital downconverter are duplicated for each element. Thus, eight identical receivers are used to provide the DSP with eight complex baseband inputs.

The reason for the single step analog downconversion and bandpass digitization is twofold. First, it is desirable to minimize the phase and amplitude unbalance between branches in the array. This is important for accurate direction finding which

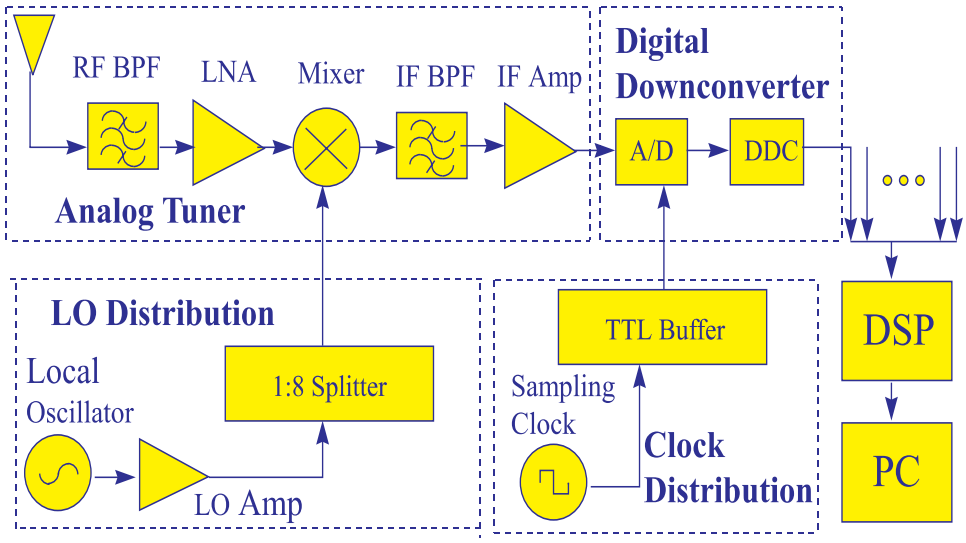

Figure 4.1: Receiver Component Block Diagram

is a secondary use of the array. The main source of unbalance between the branches is due to component variations in the analog hardware since the digital paths are nearly identically matched in phase and amplitude. Although the unbalance that can be contributed to the receiver can be calibrated out, the unbalance due to analog components tends to be temperature sensitive and thus can vary from measurement to measurement. Adding a second analog mixer and using lowpass digitization would then increase the variability of the unbalance between branches. A second analog mixer may require an additional local oscillator in the receiver. As an alternative, a single local oscillator can be used to drive both stages of mixers where the first set of mixers uses an LO frequency that is a multiple of the second LO. However, the splitters (and, possibly, doublers) required are themselves additional sources of unbalance between the branches. Secondly, it is difficult to accurately generate I and Q signals that are perfectly 90 degrees out of phase in the analog domain. In the digital domain, the I and Q mixers can be kept exactly in quadrature.

The performance specifications for the analog front end of the receivers, besides center frequency and bandwidth, are driven by two requirements. The first requirement is determined by the range of input power levels that the receiver will have to handle. The receiver needs to have a linear response over this range of input powers. This requirement essentially means the component's inherent nonlinearities, such as

intermodulation products, while always present, can be ignored over this range. One measure of the range over which the receiver's nonlinearities may be ignored is the Spurious Free Dynamic Range (SFDR) which will be discussed later. The second requirement is based on the output power levels required at the interface to the ADC. Other considerations that determine what performance specifications are reasonable to achieve include cost, power consumption and size.

The requirement for input power levels to the receiver can be quantified using link budget equations given the transmit powers allowed and the range of transmit/receive path lengths. As a first cut we can assume free space path loss with a power decay proportional to distance squared. The theoretical received power given a transmitted power, transmit and receive antenna gains and the transmit/receive path length is given by

$$P_r(dBm) = P_t(dBm) + G_t(dB) - 20log_{10}\left(\frac{4(\pi)d}{\lambda}\right) + G_r(dB) \tag{4.1}$$

For instance, for a mobile transmit power of 27 dBm with a 3 dBi gain omni directional antenna at both transmit (EIRP of 30 dBm) and receive ends and a range of distances from 5 m to 2000 m (16.4 ft to 6562 ft or 1.24 mi), the expected range of input powers to the base station receiver would be from -19.7 to -71.7 dBm assuming free space path loss. This is a 52 dB range of power levels that the receiver should be able to handle. Increasing the range of distances that might be encountered to cover from 1 m to 4000 m (3.28 ft to 13123 ft or 2.49 mi) means a range of input power levels from -5.7 to -77.7 dBm, a 72 dB range. In addition to being able to receive these power levels without going into saturation or below the minimum detectable signal, if these ranges are within the specified ranges for the application, the receiver must provide adequate signal to noise ratio to demodulate the user's signal within this range. Thus the linear range of the receiver must be greater than the expected range of input power levels. To ease this requirement, a combination of power control and automatic gain control are often used.

The second requirement is to provide the ADC with its full-scale input power and as high a signal to noise ratio as possible to make use of its full dynamic range. This requirement is challenging due to the high dynamic range ADC chosen for the multi-user spread spectrum receiver. This high dynamic range is to combat the near-far problem inherent in all multiple access wireless systems. The Analog Devices

AD9042 is a 12 bit ADC with 69 dB dynamic range between full-scale input power and the quantization noise floor for a 41 Msps sample rate without digital filtering. Furthermore, the highest spurs are specified to be 83 dB down from full-scale input power without dithering. Thus, the analog front end should be designed with a SFDR comparable to the ADC dynamic range to maximize the dynamic range of the overall receiver.

4.3 Spurious Free Dynamic Range

In determining the SFDR of the analog tuner, we must first determine the input intercept point and minimum detectable signal (MDS) of the cascaded analog components. The input intercept point of a device is the input power level at which the output intermodulation products are at the same level as the desired signal output. This intercept point is typically dominated by third order intermodulation products and thus has the notation IIP_3. These intermodulation products are due to nonlinearities inherent in the device, and in log scale, the third order intermodulation products increase at a rate three times that of the desired signal. The output power corresponding to IIP_3 normally cannot be provided by the device due to gain saturation at high input powers but is a useful theoretical measure of the linear range of a device.

The minimum detectable signal is determined by the noise floor of the device in a given bandwidth and is given as

$$NoiseFloor = kT_sB = k(NF)T_aB \tag{4.2}$$

where k is Boltzman's constant, B is the system bandwidth, T_s is the equivalent input system noise temperature, T_a is the antenna input noise temperature due to environmental noise, and NF is the noise figure of the device. The MDS is often given as 3 dB higher than the noise floor, but since we will be comparing noise floors and SFDRs of the analog tuner and ADC, we will define the minimum detectable signal to be equal to the noise floor. In linear units, the noise figure is given as

$$NF = (T_a + T_e)/T_a \tag{4.3}$$

where T_a is the standard termination noise temperature of 290 Kelvin and T_e is the effective input noise temperature of the device. The noise figure is then a measure of

the noise added by the device and can alternatively be defined as the input signal to noise ratio divided by the output signal to noise ratio.

For cascaded analog components, the NF and IIP_3 of each component must be referred to the front end for an overall NF and IIP_3 using

$$NF_{total} = NF_1 + (NF_2 - 1)/G_1 + (NF_3 - 1)/G_1G_2 + ... \tag{4.4}$$

and

$$1/IIP_3 = 1/IIP_{31} + G_1/IIP_{32} + G_1G_2/IIP_{33} + ... \tag{4.5}$$

where NF_i, G_i, and IIP_{3i} are the noise figure, gain, and input intercept point of device i respectively.

The SFDR of the overall analog tuner in log scale is then defined as

$$SFDR = 2/3(IIP_3 - MDS) \tag{4.6}$$

where IIP_3 and MDS are determined by the cascaded intercept points and noise figures given above. The low end of this dynamic range is bounded by the minimum detectable signal, and the high end is defined as the input power that brings the intermodulation products to a power equal to the noise floor. The factor of 2/3 comes from the fact that the intermodulation products increase/decrease at a rate three times that of the desired signal. Thus if the desired signal is backed off by a factor of 1/3 of the range between IIP_3 and the MDS, then the intermodulation products will decrease by a factor of 3/3 and will then be equal in power to the noise floor.

The SFDR of the analog tuner is dominated by the first amplifier's noise figure and the mixer intermodulation performance. The LNA mainly determines the overall noise figure since noise figures of later stages are divided by the gain of the previous components. Since mixers typically have the lowest input intercept points, the overall input intercept point is typically dominated by the mixer's input intercept point referred to the front end of the receiver. In the single analog IF architecture chosen, the IF amplifier has very little effect on the input dynamic range of the analog tuner. Thus, the IF gain is basically chosen to align the linear output range of the analog tuner to match the input dynamic range of the ADC.

As an example of determining the SFDR for a receiver, consider an RF BPF with 1 dB insertion loss, an LNA with a 1.5 dB noise figure and 23 dB gain, and a mixer

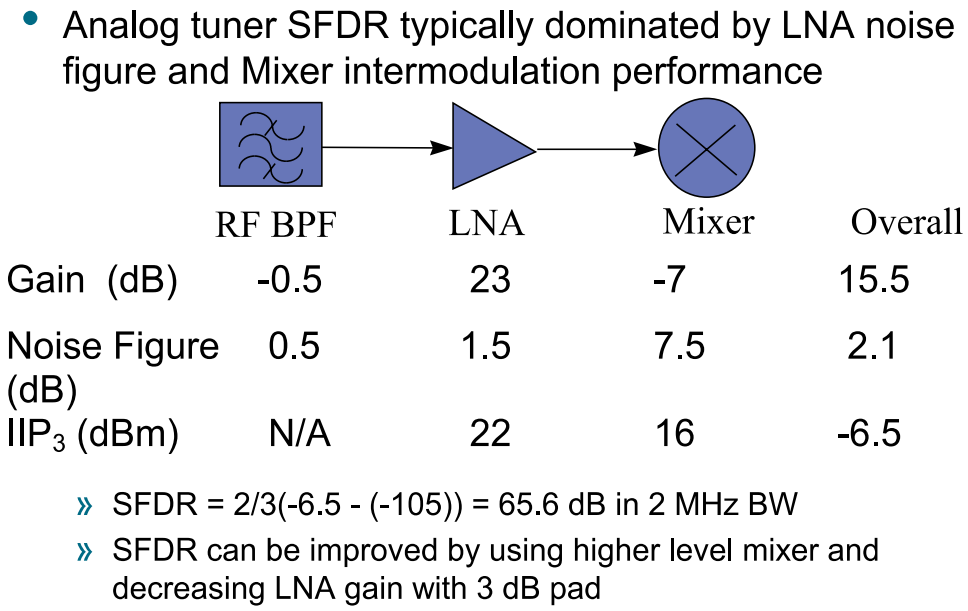

Figure 4.2: Spurious Free Dynamic Range

with an input intercept point of 16 dBm and conversion loss of 7 dB. A block diagram of this receiver is shown below.

This cascaded combination results in an overall SFDR of 70.3 dB in a 1 MHz signal bandwidth. The minimum detectable signal, defined for our case to be equal to the noise floor, is -111.4 dBm at the input to the tuner. The overall gain is 15 dB. Thus the linear input range or spurious free dynamic range of the combination is between -111.4 dBm and -44.1 dBm. Since the ADC dynamic range in a similar bandwidth is specified to be 83 dB it is the analog tuner that limits the receiver's dynamic range.

In order to increase the analog tuner's dynamic range we can increase the mixer's IIP_3 to increase the overall IIP_3 and thus dynamic range. A higher IIP_3 for the mixer requires a higher LO drive level. Going from a 7 dBm LO drive level into the mixer to a 13 dBm LO drive level gives an input intercept point of 24 dBm. The resulting SFDR is now 75.6 dB with an MDS of -111.4 dBm. Going to an even higher LO drive level mixer is impractical for the receiver since the LO signal to each mixer must be fed from the same source. An eight-way splitter induces roughly 10 dB of loss so an LO source capable of putting out at least 23 dBm is required for the level

13 mixers. This involves the use of a signal generator and a fairly expensive high power amplifier.

4.4 IF Gain Stage

In determining the IF gain required there are several considerations. These include the amount of dithering required at the input to the ADC and the amount of gain needed in the analog front end to keep the ADC's high noise figure from severely degrading the overall receiver's noise figure. Also important is the amount of gain required to provide the ADC with full-scale input power given an input RF power is important.

An ADC periodically converts the input analog waveform to a discrete digital representation. Due to the limitted number of bits the ADC has to represent the signal, there are a limitted number of discrete levels the waveform can be represented with. This leads to quantization noise which is usually considered white or of equal power across the digitized band. A dithering signal is used to provide an ADC with more input noise power than its own quantization noise to insure the quantization noise is white. As an example of why dithering is useful consider a purely sinusoidal input to an ADC with constant signal power and negligible noise power. At the peaks of the sinusoidal voltage the ADC will quantize the signal to the nearest discrete level introducing a small amount of quantization noise. However, this quantization error will be repeated identically at every signal peak and will itself be periodic. This can result in a quantization noise spur in the passband instead of the quantization noise being spread evenly across the entire digitized band. A spur in the passband can not be filtered out since it occupies the same frequency range as the desired signal. To guard against this a dithering signal can be input to the ADC with enough noise power to randomize the least significant bit of the ADC thus insuring white quantization noise. With white quantization noise further digital filtering can be used to improve the signal to noise ratio since the signal bandwidth is only a portion of the entire digitized band.

In providing a dither signal, it is necessary to provide more noise out of the analog tuner than the ADC's quantization noise. However, the quantization noise is spread across the entire digitized band while the analog tuner's noise is concentrated

in the IF passband due to analog filtering. Since oversampling is used to provide reasonable IF bandpass filters, the IF passband is fairly narrow compared to the overall digitized band. Thus, to provide more noise power out of the analog tuner than the quantization noise, the power spectral density of the analog tuner noise in the passband will be significantly higher than the power spectral density of the quantization noise in the passband. After digital filtering to isolate the passband the analog tuner noise power will be significantly higher than the quantization noise. Since the analog tuner SFDR is comparable to the ADC SFDR, making the analog tuner's noise floor higher than the ADC's is a waste of overall dynamic range since the high end of the analog tuner's dynamic range will be above the ADC's full scale power and will be for the most part unusable. An alternative is to provide a dithering signal outside the passband using a summing node before the ADC. Then the advantage of increasing the dynamic range of the ADC is achieved with the dither signal, but this dithering will be filtered out digitally so that the output noise floors of the ADC and analog tuner can be alligned to maximize the overal receiver dynamic range. With the highest spur from the ADC specified to be 83 dB without dithering and 90 dB with dithering, no dithering signal will be provided in this design since the analog tuner's SFDR is already less than the ADC's. This means the IF gain can be chosen to give full-scale input power to the ADC (4 dBm) and the dithering requirement will be neglected.

As an example of choosing the amount of IF gain needed, consider the above example. For the level 13 dBm LO drive level mixer the SFDR is 75.6 dB with a MDS of -111.4 dBm and an overall gain of 15 dB. To find the high end of the input dynamic range we take the MDS and add the SFDR. This results in a high end of the linear region of the receiver of (-111.4 + 75.6) or -35.8 dBm. To get this input level to near full-scale input power at the ADC (3 dB backoff from 4 dBm full-scale input power to guard against clipping) requires 1 - (-35.8) or 36.8 dB of gain in the IF stage. This would provide near full-scale input power to the ADC for signals at the high end of the linear region at the input to the analog tuner.

4.5 Automatic Gain Control

If it is desired to have near full-scale input power to the ADC for a range of input powers, then automatic gain control can be used at the IF gain stage. In this scenario, enough IF gain will be provided to amplify the signal level to 1 dBm at the input to the ADC regardless of the input RF power. However, this approach does not significantly affect the input dynamic range since this is mainly determined by the LNA noise figure and gain and the mixer's IIP_3.

To create a larger linear input range, automatic gain control can be implemented at RF by varying the gain of the LNA. With this approach the instantaneous SFDR will still be approximately 70 to 75 dB, but this range can be shifted up or down depending on received signal levels. This results in an overall dynamic range that is higher than the instantaneous dynamic range. The overall dynamic range is defined using the lowest noise figure possible, found when the LNA gain is turned all the way up, and the highest input intercept point, found when the LNA gain is at its minimum. Calculations show that overall dynamic ranges of roughly 95 dB are reasonable by varying the LNA gain over a range of roughly 30 dB. The simplest approach to varying the gain of either the LNA or the IF amplifier is to follow the amplifier with a variable attenuator.

As an example of the effect of changing the LNA gain, consider the following receiver. The RF stage consists of an RF BPF with 1 dB insertion loss followed by a 23 dB gain LNA with a 1.5 dB noise figure and 22 dBm IIP_3. The LNA is followed by a variable attenuator that can be varied from 0 dB to 30 dB attenuation. The next component is a level 13 mixer with a 7 dB insertion loss, 7.5 dB noise figure, and 24 dB IIP_3. The IF stage consists of a 3 dB pad for VSWR matching between the mixer and filter, an IF BPF with 10 dB insertion loss and an IF amplifier with 34 dB gain, 4.6 dB noise figure and 33 dBm IIP_3. With 10 dB attenuation in the RF attenuator, the SFDR is 75.1 dB. The overall NF is 13 dB corresponding to a MDS of -101 dBm in a 1 kHz bandwidth. This signal bandwidth is relevant to the GloMo specifications for spread spectrum transmissions. The high end of the dynamic range at the input is at (-101 + 75.1) or -26 dBm. With an overall gain of 26 dB the high end output to the ADC is 0 dBm. Without the 3 dB pad in the IF stage this output would be 3 dBm to the ADC.

Using a combination of RF and IF gain to vary the input dynamic range and provide full-scale input power to the ADC at all times is the best approach to automatic gain control. This approach is more complicated to implement than a single stage of AGC and requires more variable gain components, which are relatively expensive. To accomodate AGC, a high gain LNA was chosen to allow a variable gain attenuator to be placed behind the LNA. In the initial implementation, however, a fixed attenuator will be placed behind the LNA since the demonstrations will not require such a broad range of transmit/receive distances.

4.6 Filtering Requirements

Three stages of filtering will be used to isolate the frequency range of interest for input to the DSP. The first stage is at RF, the second at analog IF, and the third and tightest filtering is incorporated in the digital downconversion to complex baseband. The IF frequency was chosen to correspond to the center of the $4F_s$ to $4.5F_s$ band where the sample rate F_s was chosen to be 16 MHz. The sample rate of 16 MHz was chosen to be a multiple of the 1 Mcpc chip rate for GloMo and to provide roughly 8 MHz of bandwidth for an analog filter to pass a 2 MHz signal and attenuate the aliasing frequencies outside of the 8 MHz range. From filter catalogs it was found that a fifth order coaxial filter could provide approximately 50 dB aliasing attenuation outside an 8 MHz band centered at 68 MHz with a 2 MHz passband.

The RF filtering is used to limit the signals present at the input to the LNA to keep undesired interference from saturating the first gain stage. Additionally, the RF filter must sufficiently attenuate the image frequency of the analog mixer. Image frequency components that are present at the input to the mixer will be mixed to the IF passband and can limit the dynamic range of the receiver.

For an RF frequency of 2050 MHz and an IF of 68 MHz, the LO input to the mixer will be at (2050 - 68) = 1982 MHz for low side mixer injection (LO below RF). The image frequency is then at (2050 - 2(68)) = 1914 MHz or 136 MHz below carrier. Unfortunately, this image frequency falls in the unlicensed PCS band, so a high amount of attenuation here is desired. Furthermore, the insertion loss of the RF filter, which generally increases with increasing filter order, must be small since attenuation before the LNA adds directly (in dB) to the overall NF of the receiver.

Cavity resonator filters were found from Trilithic that could provide bandwidths in the 1 to 3 percent bandwidth range at 2050 MHz in a third order Chebychev response. This means relatively low insertion loss, less than 1 dB, with a 3 dB bandwidth in the 62 to 21 MHz range. With a 3 dB bandwidth of 35 MHz, the image frequency is nearly four times the 3 dB bandwidth below center frequency, and a 45 dB attenuation level at this frequency is achievable. Furthermore, the cost of these filters is less than $ 200 per piece, which is not prohibitive.

The IF filters are needed to keep undesired mixer spurious products, RF and LO mixer leakage, and out-of-band noise from aliasing into the passband during the ADC process. This aliasing can limit the dynamic range of the receiver in a similar manner to the image frequencies at RF. Furthermore, the IF filter must provide a linear phase and amplitude response over the signal bandwidth to guard against signal distortion. This requirement is less stringent in the RF filter since the signal passband is a narrow range with respect to the RF filter passband. It is desirable to oversample the IF signal somewhat to allow the IF filter room to attenuate the aliasing frequencies but not tightly filter the passband. In other words, it is desirable for the signal passband to be well within the 3 dB bandwidth of the IF bandpass filter so the filter's amplitude and phase linearity, which worsens near the passband edges, does not significantly distort the incoming waveform. High order digital filtering can be used for isolating the passband in the digital downconversion.

Following an analog mixer with a filter leads to the mixer outputing equal power at the RF - LO and RF + LO frequency. Although the desired IF in our case is RF - LO and so the RF + LO output should be rejected by the IF BPF, if the filter does not provide a 50 ohm match at the RF + LO frequency a high VSWR at this frequency will result. This means much of the signal power at this frequency will be reflected back into the mixer where it can again interact with the RF and LO frequencies and lead to undesired intermodulation products that can possibly fall in the IF passband. Thus, a diplexer is often used to allow signals to pass from the mixer to IF BPF but to highly attenuate signals in the other direction. Alternatively, a 3 or 6 dB pad can be used to help match the mixer output impedance to the IF BPF input impedance across a broad frequency range.

The IF of 68 MHz was chosen for a 1 MHz RF signal bandwidth and a sampling rate of 16 MHz. This corresponds to a 33.33 kbps data rate with a spreading factor

of 15 for a 500 kHz chip rate. This degree of oversampling is required to allow an achievable IF filter response to be specified. The IF is at 4.25 times the sampling rate. Thus the first image in the digital domain will be at 0.25 times the sampling rate or 4 MHz. With a single ADC at the IF the aliasing band is outside 4.0 and 4.5 times the sampling rate. Thus the IF filter must pass a 1 MHz signal and provide a high degree of attenuation outside an 8 MHz bandwidth. To support higher data rates a 2 MHz IF filter passband was chosen. A fifth order LC filter was found with roughly 10 dB insertion loss and 45 dB attenuation by the aliasing band edges.

This choice of IF, sample rate, and filter bandwidth can support data rates of roughly 32 kbps and 64 kbps. Furthermore, the receiver can support a data rate of 128 kbps by doubling the sample rate and going to an IF filter centered at 72 MHz with a passband of 5 MHz. No other hardware modifications are needed to support this higher data rate. The higher sample rate is needed to allow an achievable IF BPF to be specified. Standard LC or coaxial resonator filters were found for the 72 MHz IF that could achieve 45 dB aliasing rejection with the 5 MHz bandwidth. Alternatively, a SAW filter can be used, which has extremely good signal selectivity and would allow the 128 kbps to be used with a 16 MHz sample rate. However, 20 to 30 dB insertion loss is not uncommon for a SAW filter, which means an additional IF amplifier would be required to get the desired signal power at the input to the ADC.

4.7 Choice of Components

The Glomo receiver is intended to be a proof of concept to demonstrate both an adaptive beamformer and alternatively a multi-user spread spectrum base station receiver. Connectorized components were chosen to quickly develop the hardware necessary to demonstrate the adaptive signal processing techniques proposed for this project. The hardware itself is thus a prototype and is not designed for optimum size or power consumption. An integrated printed circuit board (PCB) design could significantly reduce the size and possibly power consumption of the receiver. A PCB approach, though, would take considerably more time and experience in PCB design than purchasing connectorized components. After the advantages of the adaptive signal processing are demonstrated, a more integrated approach to the hardware design will be considered.

The LNA, mixer, and IF amplifier chosen are standard Mini-Circuits components. The LNA chosen is the ZEL-1724LN. This amplifier has a NF of 1.5 dB, gain of 23 dB, input intercept point of 22 dBm, and maximum output power of 10 dBm at the 1 dB compression point. The mixer used is the ZEM-4300MH. This mixer has an input intercept point of 24 dBm, requires a 13 dBm LO drive level, has 7 dB of insertion loss, and roughly 7.5 dB noise figure. The IF amplifier used is the ZFL-1000H. This has roughly 34 dB of gain, 4.6 dB noise figure, and input intercept point of 33 dBm. Its maximum output power is 20 dBm.

The RF and IF bandpass filters were purchased from Trilithic, Inc. The RF bandpass filter is a third order 1/4 wave cavity resonator centered at 2050 MHz with a 35 MHz 3dB passband. The filter has just under 1 dB of insertion loss and provides at least 45 dB of attenuation at the image frequency. The IF bandpass filter is a fifth order LC filter with a 2 MHz 3dB bandwidth centered at 68 MHz. This filter has 10 dB insertion loss and 40 dB attenuation by the aliasing band edges at 64 and 72 MHz.

The variable attenuator between the LNA and mixer for automatic gain control will initially be replaced by a fixed 10 dB pad. A fixed 3 dB pad has also been chosen for matching between the mixer and IF BPF. Both of these attenuators are HP8493A fixed coaxial attenuators. Variable attenuators to operate in the 2 GHz band are also avialable from HP and other vendors.

The overall performance specifications for the receiver given these components is shown in the table below.

Component	NF(dB)	Gain(dB)	$IIP_3(dBm)$
RF BPF	1.0	-1.0	N/A
LNA	1.5	23	22
Attenuator	10	-10	N/A
Mixer	7.5	-7	24
IF BPF	10	-10	N/A
IF Amp	4.6	34	33
Overall	13	26	11.7

The MDS for the receiver is -101 dBm, and the IIP_3 is 11.7 dBm. Thus the SFDR is 2/3(11.7 - (-101)) = 75.1 dB. The upper end of the SFDR at the input to the receiver is (-101 + 75.1) = -25.9 dBm.

The LO distribution consists of a high power amplifier, the Mini-Circuits ZHL-42, with 30 dB of gain and a maximum output power of 28 dBm. This will be fed by an HP8648C frequency synthesized signal generator. The eight-way splitter is a Mini-Circuits ZB8PD-2 with roughly 10 dB insertion loss and a phase unbalance between outputs of less than 18 degrees. This will be the greatest source of phase unbalance between the array branches but should be accounted for in the array boresight calibration.

The digital hardware consists of an Analog Devices AD9042 ADC and a Harris HSP50016 quadrature digital downconverter. Both of these chips are available with evaluation boards. The AD9042 is a 12 bit device with an 83 dB SFDR, a maximum sample rate of 41 Msps and a maximum RF input freuqency of 80 MHz. This ADC is well suited for bandpass digitization. The Harris DDC is a 16 bit device with maximum input sample rate of 52 Msps and decimation rates in the range of 64 to 131,072. This DDC will be used for narrowband testing of the array including direction finding experiments. An alternative DDC component will be used for the GloMo receiver since the minimum sample rate of the HSP50016 is too high. Two alternatives being considered for the DDC without high decimation rates are the Analog Devices AD6620 and the Harris HSP50110.

Modifying the design for use in an ISM band at 900 or 2400 MHz would involve a different choice of LNA, RF BPF, and IF BPF. For instance, Mini-Circuits ZHL-0812LN or ZHL-0812HLN would be appropriate choices for the LNA in the 900 MHz ISM band depending on the gain required. The RF filter should be chosen to provide adequate image rejection and the IF BPF should be at a suitable center frequency determined by the sample rate.

Chapter 5

Hardware Implementation

5.1 Overview

This chapter details the implementation of the Multi-Sensor Testbed hardware. This test bed consists of eight identical receivers that interface to a DSP where adaptive beamforming is performed. This hardware was funded under the GloMo contract for innovative spread spectrum communications.

The testbed can be considered as three separate sections: the analog front end, the digital conditioning section, and the adaptive signal processing section. The LO and clock distribution systems are considered part of the analog front end and signal conditioning sections, respectively. Figure 5.1 below shows the block diagram of the receiver from RF input to baseband processing and display.

The analog front end consists of off-the-shelf MiniCircuits parts with standard 50 ohm impedances and SMA connectors. The RF and IF bandpass filters are custom Trilithic components also with SMA connectors. These parts were chosen in order to cut development time for the testbed. The digital conditioning section is composed of evaluation boards available from the manufacturers for the Analog Devices AD9042-EV analog to digital converter and Harris HSP50016-EV quadrature digital downconverter ASIC. These evaluation boards also help cut down on the development time for the testbed since the digital buffering, power, and clock connections are already in place on the evaluation boards for the AD9042 and HSP50016 chips. The signal processing is done on the decimated complex baseband outputs of each receiver chain using a single Analog Devices AD21020 DSP EZlab evaluation board.

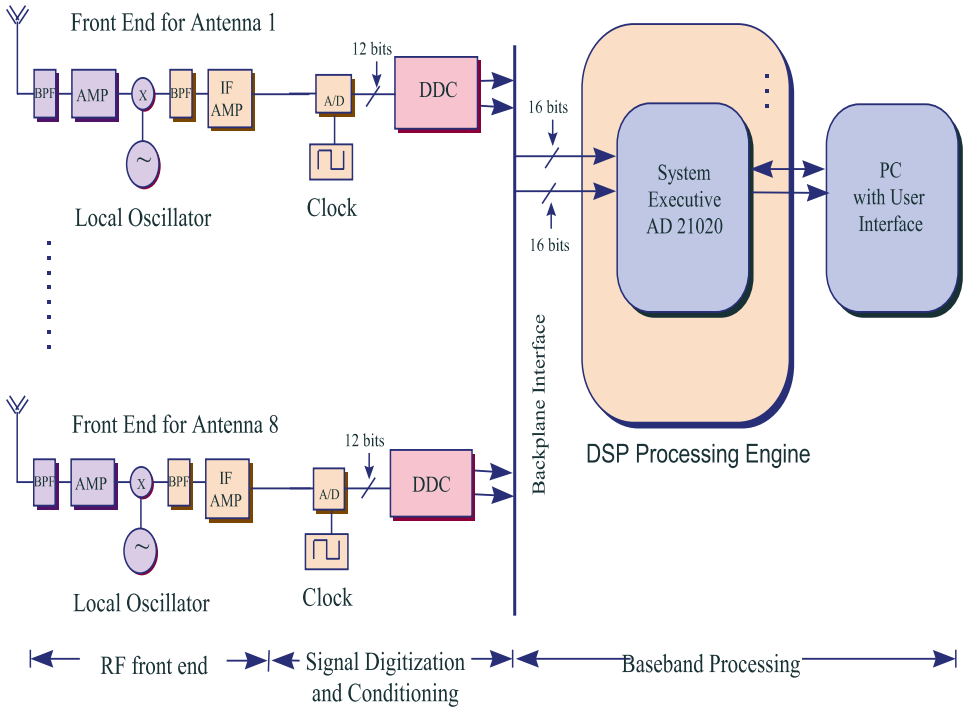

Figure 5.1: Receiver Functional Block Diagram

Again, the clock distribution, data and program memory, and data and program buses are already wired on this evaluation board as well as an interface to a PC for downloading code and uploading captured data. The testbed is not optimized for size or power consumption but is meant to be a proof of concept of a multi-channel digitizing receiver for adaptive signal processing applications. In addition it can be used to collect data for improved channel models and to perform direction finding for position location experiments.

5.2 Analog Front End

The analog front end is driven by a custom-made linear array of eight quarter wavelength monopoles mounted on a ground plane. The ground plane is roughly 12" by 24" and is supported by four 6" high legs at the corners. This support is intended to allow the antenna to stand over the analog components to allow short cable runs, roughly 12", between the antennas and the inputs to the RF BPFs. The antenna spacing is uniform with one half wavelength between each element. At 2050 MHz, this correspond s to 7.3 cm or roughly 3". Relcom single pole double throw (SPDT) solenoid switches were purchased to put between the antenna elements and the inputs to the RF BPFs. These switches are to be used for calibrating the array without having to remove and reconnect any cables. With the switches in the failsafe mode (no voltage applied), the antenna input to the switch is fed to the common port, which connects to the RF BPF input. With the voltage applied to the switches the calibration port is connected to the common port and thus the input to the filters. In this calibration mode, the antenna outputs are terminated in the switch to a 50 ohm load. This mode is used to calibrate the array by feeding a 2050 MHz tone to a 1 by 8 MiniCircuits ZB8PD-4 splitter. The splitter outputs are fed through the switches to the RF bandpass filters. By measuring the phase and amplitude unbalance between the baseband outputs of the receiver, the relative unbalance due to the receiver can be measured. This procedure is called boresighting the array and should be done before every direction finding measurement. This is important since the analog front end contribution to the phase unbalance between branches may vary due to temperature and mechanical strain on connectors. Since this can be accounted for by boresighting the array it should be done on a regular basis. Computing the array manifold as

discussed in Chapter 3 is more time comsuming and tedious. This should be done before a measurement campaign, but less often than boresighting the array.

The analog components consist of Trilithic RF BPFs centered at 2050 MHz, Mini-Circuits ZEL-1724LN low noise amplifiers, Minicircuits ZEM-4300MH double balanced mixers, Trilithic IF BPFs centered at 68 MHz with 2 MHz 3 dB bandwidth, and ZFL-1000H IF amplifiers to adjust the signal level to the desired range of the ADC. The LNA and IF amplifiers run on 15 volts DC, and the power consumption per channel was measured at 3.8 watts giving a combined power consumption of 30.4 watts for the eight-element analog front end. The analog components from the LNA to the IF amplifier have been mounted on a metal plate approximately 17" wide by 12" long for improved grounding and mechanical support for the eight analog branches. The power connections are run below the board to a shared breakout connector with leads for connection to the 15 volt DC power supply.

The LO signal for the mixers must be driven from a single source to keep the phase relationship between the branches constant. An HP 8648C signal generator is used to generate the 1982 MHz LO signal. The mixers require a 13 dBm drive level, and the 1 to 8 MiniCircuits ZB8PD-2 splitter has roughly a 10 dB loss. A Minicircuits power amplifier was purchased to amplify the LO signal before the splitter due to the limited output power of the signal generator. A drive level of -7 dBm at the signal generator was found to be appropriate for the amplifier to provide the 23 dBm drive level required at the input to the splitter. The amplifier also runs on 15 volts DC and was found to draw approximately 12 watts of DC power.

Tests were run on the analog front end to determine the noise figure and third order input intercept point of each chain. The procedure and results can be found in Chapter 6. The results showed an SFDR of 65 dB in a 2 MHz IF bandwidth. This is 5 dB less than the theoretical value but is reasonable considering additional losses in input cabling before the LNA. With tighter digital filtering of 20 kHz, this dynamic range can reach 85 dB, which is comparable to the dynamic range of the 12 bit ADC chosen for the receiver.

5.3 Analog to Digital Converter

The analog to digital converter (ADC) chosen was the 12 bit AD9042. This device is clocked at 16 MHz to digitize an 8 MHz band centered at 68 MHz. Although the maximum sample rate allowed with the AD9042 is 41 Msps, the maximum analog input frequency is 105 MHz. This means the analog sample and hold amplifiers used to limit the sampling jitter on the front end of the ADC have a wider bandwidth than required for baseband digitization using the maximum sample rate of the AD9042. This apparent over-specification makes the AD9042 well-suited for bandpass digitization where an image of the sampling process is used to digitize at an IF frequency. With a 16 MHz clock, the ADC typically is used to digitize frequencies from 0 to 8 MHz or 8 MHz to 16 MHz. Using bandpass digitization, though, the ADC can alternatively capture the band from 16 to 24 MHz or 24 to 32 MHz using the first image of the sampling process. Since the sampling process can be considered to be an impulse train in the time domain multiplied by the incoming waveform, the frequency domain interpretation is an impulse train convolved with the transfer function of the incoming waveform. This results in an image of the band from 16 to 24 MHz aliasing into the resulting 0 to 8 MHz digitized spectrum. The 24 to 32 MHz band will also alias into the 0 to 8 MHz digitized spectrum but will additionally undergo spectral reversal. Extending this process allows the ADC to digitize an 8 MHz band at 68 MHz using the fourth image of the sampling process. With the 2 MHz analog IF filters centered at 68 MHz, the filtering provides roughly 60 dB of aliasing attenuation before the aliasing band edges at 64 and 72 MHz.

If the sampling process were truly an impulse stream multiplied by the incoming waveform, there would be no limit to the order of image chosen to digitize the incoming spectrum, except the limit of the maximum frequency the input sample and hold amplifiers could handle. Since, however, the sampling instant has finite duration, this natural sampling leads to a Sin(x)/x distribution overlaid on the sampling impulse train in the frequency domain. This leads to an additional limitation to bandpass digitization in addition to the limits of the input analog amplifiers. Higher order images will mix to the 0 to $F_s/2$ range but will be attenuated by the Sin(x)/x distribution. The fourth order image was not found to exhibit significant attenuation caused by the finite sampling instant.

The oscillator used to simultaneously clock the eight ADCs is a 16 MHz crystal

oscillator purchased from Oscillatek. The clock is specified to have a TTL fanout of 30. Buffering of the clock using a TTL line driver was tested, but the current drawn by the eight boards when the ADC is triggered was found to significantly distort the buffer output and cause sampling jitter. Since the clock has a relatively large fanout, the clock was tested without any buffering. This proved to decrease the amount of distortion in the clock and introduce less sampling jitter in the analog to digital conversion. The amount of jitter present is best measured with an oscilloscope triggering on an edge of the clock and set to accumulate multiple waveforms. The width of the accumulated rising edges gives a measure of the peak to peak sampling jitter present at the ADC.

Sampling jitter between the branches takes on additional significance considering it directly translates to a jitter in the phase relationship between branches of the adaptive array. When performing adaptive beamforming the algorithm will typically attempt to minimize distortion in the incoming waveform by steering nulls in the direction of interfering sources. The direction in which the null is steered is extremely sensitive to the phase relationship between the elements. Phase jitter can cause the minimum of the null (minimum gain or peak attenuation) to wander slightly around the true direction of the interfering source and limit the amount of interference rejection achieved.

Connection to the ADC from the analog front end is made using an SMA to BNC cable since the evaluation board provides a BNC connection to the analog input. A BNC connection is also available for the clock input. BNC connectorized cable is used to feed the clock to the ADC with a breakout connector clipped to clock and ground on the clock distribution circuit. The digital output of the ADC is via a 40 pin two row ribbon cable connector. Since the input to the Harris HSP50016-EV board is via a 96 pin DIN connector, custom-made ribbon cable adapters were used to transfer the digitized data from the ADC to the Harris DDC boards. The connector provides 12 bits of data, a ground connection, and a clock output. The clock output from the ADC to the DDC is used to trigger the Harris board to read the ADC's buffered output. Since the ADC clock output also clocks data into the on-board buffering chips, the clock is inverted on the Harris DDC. This introduces a half cycle delay from when the data is loaded into the ADC output buffer to when the sample is read from the buffer by the DDC. This is important when considering the 7 ns settling time

requirement on the input data lines to the Harris DDC evaluation board. Without inverting the clock, the data was measured to be stable for roughly 5 ns before the DDC is triggered to read. No significant distortions were found with this reduced settling time, but the clock was inverted anyway as a precaution.

The AD9042 chip runs on a standard 5 volt DC power supply and is specified to dissipate 625 mW of power per chip. With the evaluation board, however, the ADC was found to dissipate 4.6 watts of power per channel for a total of 36.8 watts for eight ADCs. Separate power connections are wired on the ADC evaluation board to keep the relatively noisy digital supply voltage from the analog front end of the ADC. Although this is not recommended, these supplies were wired together for simplicity. No significant distortions were detected with this approach, but this should be investigated further in the future.

5.4 Quadrature Digital Downconversion

The digitized signal is further conditioned on the HSP50015-EV quadrature digital downconversion boards before being fed to the DSP, reducing the burden on the DSP and allowing the DSP processing power to be dedicated to the adaptive algorithms. The Harris DDC has quadrature sin and cos mixers on board, a fifth order high decimation cascaded integrate and comb filter, and fixed coefficient FIR filters that further decimate the signal and compensate for passband ripple from the CIC filters. A functional block diagram of the Harris HSP50016 is shown in the Figure 5.2 below.

The quadrature mixers are composed of two real multipliers, one for the in-phase and another for the quadrature component. These multipliers are fed from an on-chip local oscillator. The phase generator of the local oscillator uses a 32 bit register resulting in a frequency resolution of

$$DDCresolution = F_{clk}/2^{N_{phaseregister}} \tag{5.1}$$

where $N_{phaseregister}$ is the number of bits in the phase register. For a sample rate of 16 MHz and a 33 bit phase register this results in a frequency resolution of 0.002 Hz for the local oscillator. This is the resolution to which the digital local oscillator frequency can be set. The 18 MSBs of the phase generator are fed to the real multipliers and the result rounded down to 17 bits. This guarantees 102 dB of SFDR through the mixers.

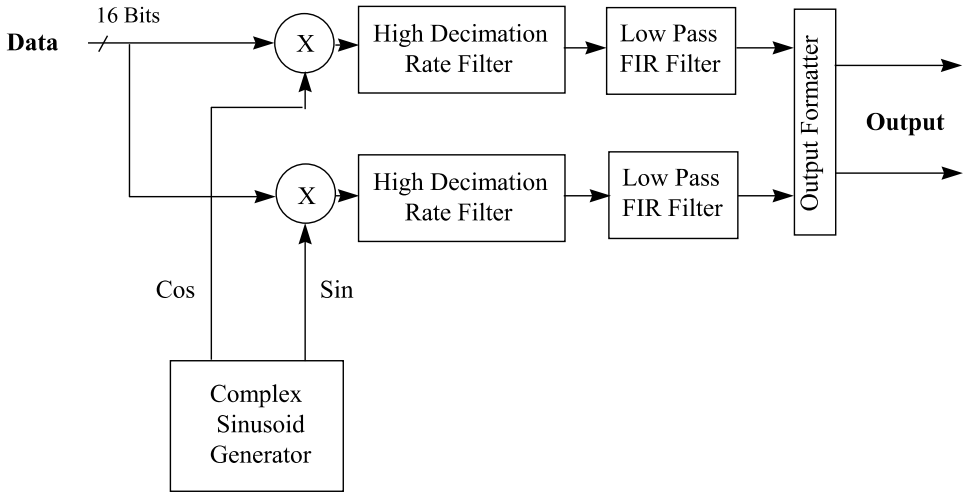

Figure 5.2: Digital Downconverter Functional Block Diagram

The next stage of High Decimation Filtering is performed by cascaded integrate and comb filters, which are fairly common for high sample rate decimating filters since the integration filter consists of only accumulators and no multipliers. The frequency response of the fifth order cascaded integration filter is given as

$$H(f) = (Sin(\pi f)/Sin(\pi f/R))^5 \tag{5.2}$$

where R is the decimation rate through the HDF section. The minimum value R can take is 16. The decimation by 4 through the output formatter leads to a minimum overall decimation rate of 64.

The HDF section is followed by an FIR filtering stage for passband roll off compensation, transition band shaping, and further aliasing attenuation before the final stage of decimation. The FIR filters are functionally equivalent to two identical 121 tap lowpass FIR filters. These filters are implemented with a single real multiplier, a sum of products accumulator, and a table of coefficients stored in ROM. The composite passband through the HDF and FIR filtering sections has a ripple of less than 0.04 dB and over 102 dB of stopband attenuation. The double sided bandwidths for the -3 dB and -102 dB points are given by the following equations

$$3dB_BW = (0.13957)f' \tag{5.3}$$

$$102dB_BW = (0.19903)f' \tag{5.4}$$

where f' is the decimated rate F_s/R, F_s is the sample rate, and R is the decimation rate of the HDF. The double sided bandwidth is appropriate since both I and Q data rates are at the decimated rate. In other words, the frequency response of the complex signal in the range from 0 Hz to $F_S/2$ Hz need not be the mirror image of the frequency response from -$F_s/2$ Hz to 0 Hz, as is the case for real signals. For a 16 MHz sample rate and minimum decimation of 16 and 4 through the HDF and FIR filtering sections, respectively, the 3 dB bandwidth is roughly 140 kHz allowing a maximum chip rate in the 70 kcps range or less. This bandwidth is wide enough for AoA measurements but is a bottleneck in terms of bandwidth for spread spectrum applications.

Control of the Harris DDCs is done over a COM port connection to a PC running the evaluation board software provided by Harris. Control consists of loading eight 40 bit words to the Harris boards at initialization to program the mixing frequency, decimation rate, output format, and other parameters. This initialization is done each time the receiver is powered up by running an automated batch file on the PC with the appropriate control words. This batch file is named init.bat and can be found on the PC in the DSP lab at MPRG.

The DDC is a 16 bit device so, since the ADC is a 12 bit device, the lower four LSBs are tied to ground to keep them from oscillating and damaging the DDC chip. The 16 bits of I and Q data are transferred to the DSP in a single 32 bit parallel data transfer. The decimated output data clock of the DDC is wired to the DSP interrupt request 1 line (IRQ1). This interrupt tells the DSP that data is ready from the DDCs. The DDCs are connected in parallel to the DSP's data memory data (DMD) lines. The output enable lines of the Harris boards are wired to the DSP. This was done to keep the Harris boards from loading data onto the DSP's DMD lines before the DSP was prepared to read the data. The Harris evaluation board has the output enable lines for its output buffers wired to a control register so they may be enabled or disable by sending the appropriate control word over the Harris board's PC interface. Since this is not feasible to do at the sample rate, it was decided to cut these control lines on the Harris board and rewire these lines to an address decoder whose inputs are tied to the DSP's data address lines. In this way, the DSP simply reads from a specified address outside the DSP's onboard data memory limits, and this address triggers the output enable of the Harris boards during the sequential reading of the Harris

boards by the DSP. Thus, when the DSP receives a strobe from the Harris boards, it sequentially enables the outputs of each DDC and reads the sample data over its upper 32 DMD lines. While the DSP is not enabling the DDC boards, their outputs are held in a high impedance state. Because the DDC boards are in parallel on the DMD bus, even with the output buffers in high impedance state, the boards were found to load the DSP's DMD lines. This results in intermittent problems with the DSP writing to its own data memory on the EZlab evaluation board over the DMD bus. To remedy this, the wait states for the DMD bus on the DSP were increased so that data is held on the bus twice as long as normal when the DSP is controlling its DMD bus.

The Harris boards were found to require 1.7 watts per board at 5 volts DC. This results in a dissipation of 13.6 watts of power for eight DDCs. The Harris evaluation boards were found to work best at 4.3 volts supply voltage when eight boards are in parallel. At higher voltages, the Harris boards tend to lose synchronization between the boards, which causes the phase relationship between chains to drift. This power is supplied via a 96 pin daisychained backplane purchased from Schroff. This backplane simplifies the interface to the DSP since the backplane provides access to all of the eight DDC boards output data lines via a single 32 bit bus. This backplane also provides a shielding plane, which was connected to ground via shorting jumpers to reduce coupling between the data lines, which are located in close proximity to one another. This coupling effectively acts as capacitance between the data lines, allowing high frequency data transition noise to leak from one data line to the next. This transition noise requires the data to be held for a longer period on the data lines to allow the data to settle before being read by the DSP. This was also remedied by increasing the wait state from 0 to 1 on the DSP reads using the DMD lines.

5.5 Digital Signal Processing

The Multi-Target CMA algorithm has been implemented on the AD21020 DSP by Paul Petrus and Steve Nicoloso. This code was modified by Nitin Mangalvedhe, Steve Nicoloso and myself to operate on an interrupt driven data basis. In addition, a real-time interface to the PC was added to display the resulting beampattern the

algorithm is using on the PC. The interface to the PC is done using a National Instruments DIO-96 digital acquisition board and the Labview software package to drive the data acquisition board and convert the uploaded weight vector to a beampattern for display. The programs required for running the real-time two-target CMA routine are targ2cma8.asm, gso.asm, cma2.asm, isqrt.asm, mprgmacs.h,

The main program is the targ2cma8.asm assembly file. This file initializes the chip, enables IRQ1 so that the DSP can respond to strobes from the Harris DDCs, and keeps counters to decide when to call the CMA routine, the Gram-Schmidt Orthogonalization (GSO) routine, and when to write weight vector words over the LabView interface. In the main routine in targ2cma, the program waits in an idle state for an interrupt on IRQ1. Upon receiving this interrupt, the program goes to the interrupt 1 subroutine and sequentially reads data values from the Harris DDCs over the DMD bus, which is brought out over a 96 pin external connector JP1 on the EZLab evaluation board for the AD21020 DSP. As mentioned above, this is done by reading from addresses defined in the EzLab21k.ach architecture file. The address lines of the data memory bus, DMA lines, are wired from the 96 pin connector JP1 to a series of nand gates that act as address decoders. Upon receiving the appropriate address for a Harris DDC, the output of one of the nand gates is held low. This output is wired through the backplane to the output enable line of the appropriate Harris DDC. In this way, the Harris DDCs data sample is put on the DSP's data memory data bus during the time the DSP reads the DMD bus. This is done eight times, one 32 bit read from each DDC, every time the DSP receives a data ready strobe from the Harris boards. These strobes occur at the decimated sample rate. Counters initialized in the targ2cma.h header file determine how often the main program calls the CMA, GSO, and Labview subroutines. These counters are checked and updated after each IRQ1. The assembly code can be downloaded to the DSP via the emulator using the makeice.bat batch file. All of these files are on the DSP lab PC at MPRG. A block diagram illustrating the two-target CMA routine is shown below.

A record of the weight vectors the two CMA algorithms have computed is stored in on-board memory on the EZlab evaluation board while the DSP is running. However, to view this record on the PC, the DSP must be halted and the contents of the on-board memory uploaded via the emulator. Similarly, test programs such as ADC8.asm have been written to store the received data from the Harris DDCs to memory for

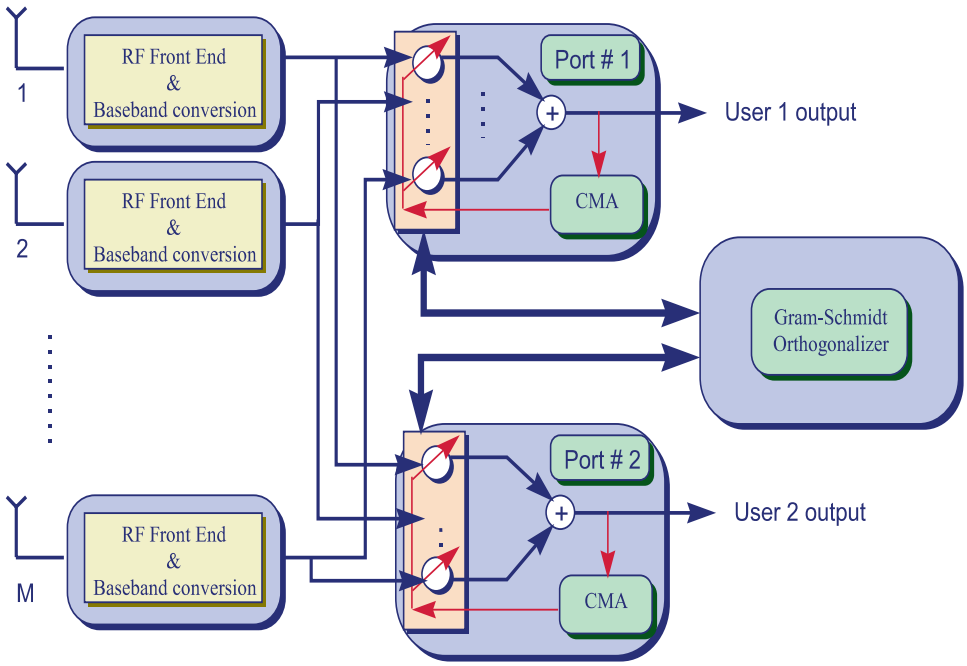

Figure 5.3: Two-Target CMA Functional Block Diagram

later uploading. These test programs can be run with tone or multi-tone inputs to the receiver to test the end to end SFDR of the combined analog and digital hardware sections.

To view the weight vectors the algorithm has computed in real time, an interface from the DSP to a digital acquisition board was developped by Francis Dominique and myself. By controlling the digital acquisition board with the LabView software package the weight vectors can be uploaded to a PC in real time. This allows the two resulting beampatterns to be computed and displayed as the DSP adapts and allows the user to gain an intuitive insight into the adaptation of the beamformer.

Chapter 6

Testing of the Analog Front End

6.1 Overview

Analog hardware testing was performed to verify first that the components met the manufacturer specifications and secondly that the cascaded chain of analog components met the design specifications for the adaptive antenna array. The testing consisted of measuring the noise figure (NF) and third order input intercept point (IIP3) of an analog chain to compute the spurious free dynamic range of the analog front end. A single chain consists of an RF bandpass filter, low noise amplifier, triple balanced mixer, IF bandpass filter, and IF amplifier.

The testing procedure consisted of measuring the individual gain of each component, measuring the overall gain of the analog chain, measuring the noise power out of the chain with a 50 ohm termination on the input for noise figure computation and finally measuring the intermodulation levels out of the chain with a two-tone input for varying input levels to determine the third order intermodulation intercept point. The equipment required included the devices under test mentioned above, two HP 8648C signal generators to provide RF signal inputs, an HP ESG-D4000A digital signal generator for the mixer LO signal, an HP 8594E spectrum analyzer for measuring output powers, various coaxial cables, BNC/SMA adaptors and connectors and a BNC T connector for combining the HP8648C outputs for the two-tone intermodulation test. A DC power supply at 15 volts was also required for the LNA and IF amplifier.

6.2 Procedure

Before measuring the individual gains of the components, the signal generators, cables, and spectrum analyzer must be calibrated with each other to decide the loss to attribute to the cables. This is important so that the actual input and output powers for the measured devices can be found from the recorded settings of signal generator power and power measured on the spectrum analyzer. After measuring the cable losses, the individual gain of each device is found by inputing a known signal level from the HP 8648C signal generator and measuring the output power with the spectrum analyzer. Since the gain of a device is the output power minus the input power, the actual gain of the device is the power measured by the spectrum analyzer minus the power output by the signal generator plus the loss in the input and output cables. The RF BPF and LNA should be measured at 2050 MHz input and output, the mixer takes a 2050 MHz RF input, an LO of 1982 MHz and the output should be measured at 68 MHz. The IF BPF and IF amplifier should be measured at 68 MHz. When measuring the gain of the mixer (insertion loss) it is important to provide the LO port with at least the specified LO drive level. For the ZEM-4300MH MiniCircuits mixer used, this LO drive level is 13 dBm. After the individual component gains are measured the overall gain of the cascaded analog chain is measured.

After measuring the gains, the next step is the NF measurement, done by attaching a 50 ohm termination to the RF filter input and measuring the output noise power in a given resolution bandwidth. The video bandwidth of the spectrum analyzer should be at least as wide as the resolution bandwidth, and video averaging should be turned off. Care must be taken to insure that the measured noise is due to the analog chain and not the spectrum analyzer's own thermal noise. This can be checked by powering up the analog chain and observing the roughly 4 MHz IF passband with the spectrum analyzer. Then the DC power should be turned off for the LNA and IF amplifier. The noise level read by the spectrum analyzer should drop by roughly 10 dB or more to insure the sprectrum analyzer's noise is not biasing the noise measurement. If the noise level does not drop by at least 10 dB, then the spectrum analyzer's attenuation level should be decreased to improve its noise figure performance. Alternatively, the spectrum analyzer's resolution bandwidth can be decreased.

Once the output noise power is measured and the resolution bandwidth recorded, the noise power should be referred to the chain's front end by subtracting the overall

measured gain of the analog front end. Given an equivalent input noise power, the system noise temperature can be computed using

$$P_n = kT_sB \tag{6.1}$$

where P_n is the equivalent input thermal noise power in watts, k is Boltzman's constant of 1.38 E-23 W/K*Hz, and B is the resolution bandwidth in Hertz used in the measurement. Given an equivalent input system noise temperature, the noise figure in linear units is found by dividing the system noise temperature by the standard source noise temperature of 290 Kelvin.

The final measurement is for the third order intermodulation input intercept point. This test uses both HP 8648C signal generators with one set at 2050MHz and the second set at 2050.01 MHz for a 10 kHz tone spacing. The two signal generator outputs are fed to the BNC T connector, and the single output is fed to the input to the reciever. As with the noise figure measurement, it is important to make sure the spectrum analyzer and signal generators are not contributing to the intermodulation products measured. First, the two tone signal should be fed directly to the spectrum analyzer, and the intermodulation products observed. The third order intermodulation products should appear with nearly equal power at the tone spacing above and below the high side and low side tones, respectively. Since the spectrum analyzer's front end attenuation level affects its intermodulation performance, increasing this attenuation should decrease the intermodulation products. If the products are not affected by the attenuation level or if they are asymmetric, fixed attenuators should be placed at the output of one or more of the signal generators.

Next the two tone signal should be fed to the analog chain, and the output observed with the spectrum analyzer. To insure the intermodulation products are due to the receiver, again vary the spectrum analyzer attenuation level. The products can be attributed to the receiver if increasing the spectrum analyzer's attenuation level does not decrease the intermodulation levels. Next the individual tone output powers and intermodulation products output powers should be recorded for varying input powers. The input power should be swept over at least a 10 dB range. MATLAB can then be used to plot the input power versus output power for the tones and input tone power versus output intermodulation power for the strongest intermodulaton product. A least squares fit is then found for a first order polynomial for both tones and intermodulation products and the intersection of these lines is the input intercept

Table 6.1: Analog Performance Specifications

Component	Specified Gain (dB)	Measured Gain(dB)
Trilithic RF BPF	-0.9	-0.4
MiniCircuits LNA	23	25
MiniCircuits Mixer	-7	-6.2
Trilithic IF BPF	-10	-4.6
IF Amp	21.4	25.8
Overall	28.3	39.6

point of the receiver. The spurious free dynamic range in log scale is simply 2/3 the difference between the noise floor and the input intercept point in the system bandwidth.

6.3 Results

Table 6.1 shows the manufacturer specified gains and the measured values for the individual components.

The measured overall gain of the chain was 35.7 dB, roughly 4 dB less than the sum of the individual measured gains. This can partially be explained by additional losses in the connectors between devices and impedance mismatches.

For the NF measurement, a 1kHz resolution bandwidth was used, centered at 68 MHz in zero span mode. In this mode the display shows the power measured in the resolution bandwdith as a function of time. The measured power varied between -104 and -101 dBm corresponding to NF values between 4 and 7 dB respectively. The theoretical value is 3.1 dB for the cascaded chain based on the manufacturer specified gains and noise figures.

The input intercept point is found from the measured intermodulation levels by extrapolating a linear fit to the data for the input versus output tone power and input tone power versus output intermodulation levels. Figure 6.1 shows the measured levels and a least squares fit to the data. The intersection of the two lines corresponds to the input intercept point. The intercept point for the chain is approximately -11 dBm. The theoretical value is -8 dBm for the analog chain. This is based on the input

intercept point of the mixer, which typically dominates intermodulation performance, being specified at 10 to 15 dB higher than the 1 dB compression point of the mixer. For the ZEM-4300MH, the 1 dB compression point is 7 dBm for a LO drive level of 13 dBm. Thus the input intercept point should be between 17 and 22 dBm. The value of 17 dBm was used for the mixer to compute the -8 dBm theoretical overall input intercept point of the cascaded chain since this value is appropriate above the mid-frequency range of the mixer. Since the overall intercept point is 3 dB lower than expected, the true intercept point of the mixer is most likely near 14 dBm. Alternatively, intermodulation products due to the spectrum analyzer and signal generators may have biased the measured values although precautions were taken to minimize these effects.

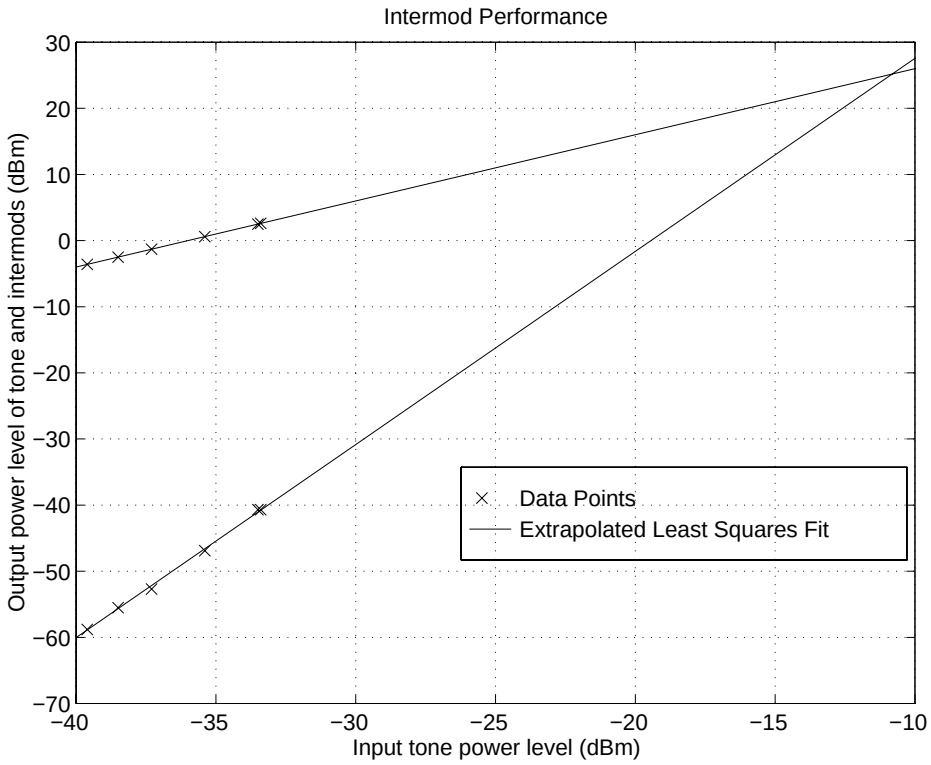

Figure 6.1: Intermodulation Performance of Analog Chain

Based on a measured NF of approximately 5 dB, the noise floor is -109 dBm at the input to the receiver in a 1 MHz bandwidth. For a -11 dBm IIP_3, the SFDR is then 2/3*(-11 -(-109)) or 65 dB. The SFDR at the input to the chain is then from -109

dBm to -44 dBm. This corresponds to an output range from -73 dBm to -8.3 dBm. As suggested in the final design, replacing the IF amp ZFL-2000 with a ZFL-1000H amplifier would increase the overall gain by 10 dB and would align the high end of the analog chain's SFDR with the ADC's high end. The theoretical value for the SFDR based on the manufacturers specifications for the components is 69 dB.

6.4 Conclusions

The measured performance of the analog chain in general agrees with the theoretical performance given the manufacturer's specifications for the individual components. The NF is slightly higher than expected, but adding small amounts of loss for connectors and impedance mismatches at the front end of the analog chain could account for the difference in the measured and theoretical values. Likewise, the input intercept point is slightly lower than expected. The overall measured SFDR is 4 dB less than expected but is reasonably close considering measurement inaccuracies, unexpected losses, and a slighlty lower intercept point than specified by the manufacturer.

Chapter 7

Conclusions

7.1 Future Work

The two most important tasks left to complete in the testbed hardware development are to put the array in a more portable and rugged format and to calibrate the array for channel measurements. A 19" three-tier rack was purchased to consolidate the hardware and make it more portable. Backplanes also need to be added to make the ADC and DDC portion of each receiver chain a single unit. Calibration must be done to measrue the array manifold, and an automated boresighting procedure needs to be developed using the SPDT switches purchased.

Extensions to the array include a wider bandwidth version based on the Harris HSP50214 wideband DDC and the Sigtek ST-114 evaluation board for this DDC. These boards make it possible to test wider bandwidth applications such as spread spectrum multiple access systems and combined spatial and temporal channel sounding.

7.2 Conclusions

The use of adaptive antenna arrays shows promise for improving the capacity of wireless systems and for providing improved safety through position location capabilities. While many technical challenges exist today for employing this technology, the use of adaptive antenna arrays has yet to reach its full commercial potential. Constant advances in computing capabilities for DSPs and advances in high speed ADCs have

made flexible software radios and adaptive beamforming in digital signal processing realizable today. The Multi-Sensor Tesbed is meant to be a platform to explore the applications of adaptive signal processing in the spatial domain. Potential applications include spatial filtering for interference rejection and capacity improvements, position location through direction finding measurements, and improved channel moodels that include measured angle of arrival statistics.

The Testbed in its current state is set to run a two-target adaptive beamforming algorithm to show the capabilities of the CMA algorithm to separate two co-channel users at high interference levels through spatial filtering. Numerous classes of adaptive beamforming algorithms can be compared in live channel conditions, and the limitations of receiver performance on beamforming can be explored with this testbed. In addition, the array can be set to capture data in roughly 120 kbytes of program and data memory. This data can be processed after uploading to a PC for applications of MUSIC or alternative direction finding algorithms. Variaitons of the Geometrically Based Single Bounce Channel Model [15], [16] can be tested for accuracy through extensive data collection campaigns. A wider bandwidth version of the array can be used to explore combined spread spectrum and adaptive beamforming applications. All of these applications must be demonstrated and verified to show industry leaders that adaptive antenna arrays, and software radios in general, have unrealized commercial potential.

Bibliography

[1] D. Wayne, "Wireless e911 available in steps under joint plan", *Radio Communications Report*, p. 3, February 1996.

[2] D. Pearl, "Cell phones: Perfect in emergencies? try again", *Wall Street Journal*, pp. B1–B5, April 1995.

[3] Federal Communications Commission, "Cc docket no. 94-102", *Notice of Proposed Rule Making by the FCC*, 1994.

[4] C. J. Driscoll and Assocciates, *Survey of Location Technologies to Support Mobile 911*, C. J. Driscoll and Associates, Rancho Palos Verdes, CA, 1 edition, July 1994.

[5] Federal Communications Commission, "Cc docket no. 96-52", *Report and Order by the FCC*, June 1996.

[6] et. al. A., Paulraj, *Subspace Methods for Direction-of-Arrival Estimation*, vol. Chapter 16 of *Handbook of Statistics 10 - Signal Processing and its Applications*, ed. Bose, N.K., and Rao, C. R.,, 1993.

[7] W. L. Stutzman and G. A. Thiele, *Antenna Theory and Design*, John Wiley and Sons, New York, 1981.

[8] B. Widrow, "Adaptive antenna systems", in *Proc. of the IEEE*, December 1967, vol. 55, pp. 2143–2159.

[9] B. G. Agee, "The least-squares cma: A new technique for rapid correction of constant modulus signals", in *Proc. IEEE Intern. Conf. ASSP*, April 1986, pp. 953–956.

[10] B. G. Agee J. R. Treichler, "A new approach to multipath correction of constant modulus signals", in *IEEE Trans. on ASSP*, April 1983.

[11] J. R. Treichler M. G. Larimore, "Noise capture properties of the constant modulus algorithm", in *Proceedings of the ICASSP*, Boston, 1983, pp. 13–16.

[12] B. G. Agee, "Blind separation and capture of communications signals using a multitarget constant modulus beamformer", in *Proc. of the IEEE MILCOM*, 1989, pp. 340–346.

[13] R. O. Schmidt, "Multiple emitter location and signal parameter estimation", in *Proceedings of RADC Spectrum Estimation Workshop*, 1979, pp. 243–258.

[14] R. O. Schmidt and R. E. Franks, "Multiple source df signal processing: An experimental system", in *IEEE Transactions on Antennas and Propagation*, March 1986, vol. AP-34, pp. 281–290.

[15] J.C. Liberti, *Analysis of CDMA Cellular Radio Systems Employing Adaptive Antennas*, PhD thesis, Virginia Polytechnic Institute and State University, September 1995.

[16] P. Petrus, *Novel Adaptive Antenna Array Algorithms and Their Impact on Cellular System Capacity*, PhD thesis, Virginia Polytechnic Institute and State University, February 1997.

Author's Biographical Sketch

Donald Breslin was born on October 20, 1970, in Ridgewood, NJ. He received his B.S. degree in Electrical Engineering from VA Tech in 1994. From 1995 to the present, he has worked as a graduate research assistant for the Mobile and Portable Radio Research Group. His research interests include receiver design and digital signal processing for adaptive antenna arrays.